

1 Extreme heterogeneity of influenza 2 virus infection in single cells

3 Alistair B. Russell¹, Cole Trapnell², Jesse D. Bloom^{1,2*}

*For correspondence:
jbloom@fredhutch.org

4 ¹Basic Sciences Division and Computational Biology Program, Fred Hutchinson Cancer
5 Research Center, Seattle, United States; ²Department of Genome Sciences, University of
6 Washington, Seattle, United States

7

8 **Abstract** Viral infection can dramatically alter a cell's transcriptome. However, these changes
9 have mostly been studied by bulk measurements on many cells. Here we use single-cell mRNA
10 sequencing to examine the transcriptional consequences of influenza virus infection. We find
11 extremely wide cell-to-cell variation in the productivity of viral transcription – viral transcripts
12 comprise less than a percent of total mRNA in many infected cells, but a few cells derive over half
13 their mRNA from virus. Some infected cells fail to express at least one viral gene, but this gene
14 absence only partially explains variation in viral transcriptional load. Despite variation in viral load,
15 the relative abundances of viral mRNAs are fairly consistent across infected cells. Activation of
16 innate immune pathways is rare, but some cellular genes co-vary in abundance with the amount of
17 viral mRNA. Overall, our results highlight the complexity of viral infection at the level of single cells.

18

19 Introduction

20 Viruses can cause massive and rapid changes in a cell's transcriptome as they churn out viral mRNAs
21 and hijack cellular machinery. For instance, cells infected with influenza virus at high multiplicity
22 of infection (MOI) express an average of 50,000 to 100,000 viral mRNAs per cell, corresponding
23 to 5 to 25% of all cellular mRNA (Hatada et al., 1989). Infection can also trigger innate-immune
24 sensors that induce the expression of cellular anti-viral genes (Killip et al., 2015; Iwasaki and Pillai,
25 2014; Crotta et al., 2013). This anti-viral response is another prominent transcriptional signature of
26 high-MOI influenza virus infection in bulk cells (Geiss et al., 2002).

27 However, initiation of an actual influenza infection typically involves just a few virions infecting
28 a few cells (Varble et al., 2014; Poon et al., 2016; Leonard et al., 2017; McCrone et al., 2017). The
29 dynamics of viral infection in these individual cells may not mirror bulk measurements made
30 on many cells infected at high MOI. Over 70 years ago, Max Delbrück showed that there was a
31 ~100-fold range in the number of progeny virions produced per cell by clonal bacteria infected
32 with clonal bacteriophage (Delbrück, 1945). Subsequent work has shown similar heterogeneity
33 during infection with other viruses (Zhu et al., 2009; Schulte and Andino, 2014; Combe et al., 2015;
34 Akpinar et al., 2016), including influenza virus (Heldt et al., 2015).

35 In the case of influenza virus infection, targeted measurements of specific proteins or RNAs
36 have shed light on some factors that contribute to cell-to-cell heterogeneity. The influenza virus
37 genome consists of eight negative-sense RNA segments, and many infected cells fail to express
38 one more of these RNAs (Heldt et al., 2015; Dou et al., 2017) or their encoded proteins (Brooke
39 et al., 2013). In addition, activation of innate-immune responses is inherently stochastic (Shalek
40 et al., 2013, 2014; Bhushal et al., 2017; Hagai et al., 2017), and only some influenza-infected cells
41 express anti-viral interferon genes (Perez-Cidoncha et al., 2014; Killip et al., 2017). However, the
42 extent of cell-to-cell variation in these and other host and viral factors remains unclear, as does the

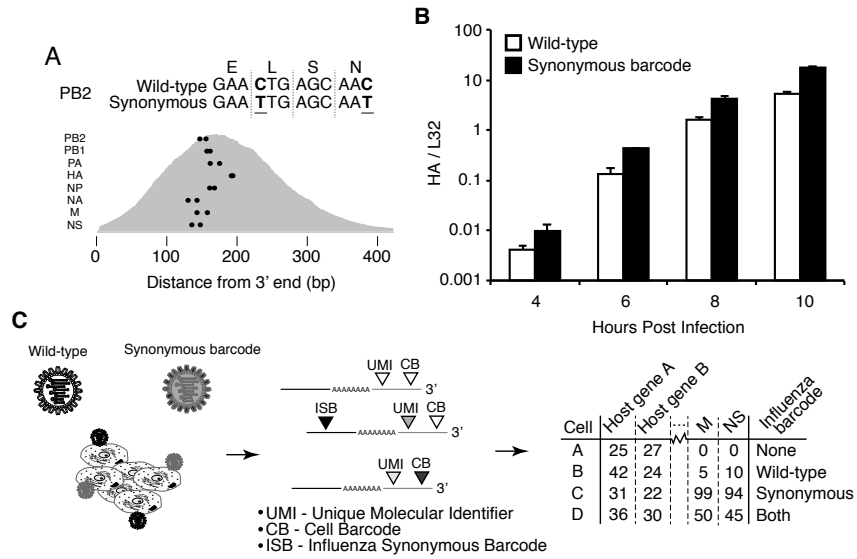


Figure 1. Experimental design. **(A)** We engineered a virus that carried two synonymous mutations near the 3' end of each mRNA. At top are the mutations for PB2. At bottom are locations of the synonymous mutations relative to the typical distribution of read depth for our 3'-end sequencing. **(B)** The wild-type and synonymously barcoded viruses transcribe their genes with similar kinetics. The abundance of the viral hemagglutinin (HA) transcript relative to the cellular housekeeping gene L32 was assessed by qPCR in A549 cells infected at an MOI of 0.5 (as determined on MDCK-SIAT1 cells). Error bars \pm S.D., n=3. **(C)** For the single-cell mRNA sequencing, A549 cells were infected with an equal mixture of wild-type and synonymously barcoded virus. Immediately prior to collection, cells were physically separated into droplets and cDNA libraries were generated containing the indicated barcodes. The libraries were deep sequenced, and the data processed to create a matrix that gives the number of molecules of each transcript observed in each cell. Infected cells were further annotated by whether their viral mRNAs derived from wild-type virus, synonymously barcoded virus, or both.

Figure 1-source data 1. Sequences of wild-type and barcoded viruses are in [viralsequences.fasta](#).

43 association among them in individual infected cells.

44 Here we use single-cell mRNA sequencing to quantify the levels of all cellular and viral mRNAs
45 in cells infected with influenza virus at low MOI. We find extremely large variation in the amount
46 of viral mRNA expressed in individual cells. Both co-infection and activation of innate-immune
47 pathways are rare in our low-MOI infections, and do not appear to be the major drivers of cell-
48 to-cell heterogeneity in viral transcriptional load. Individual infected cells often fail to express
49 specific viral genes, and such gene absence explains some but certainly not all of the cell-to-cell
50 heterogeneity. A variety of cellular genes, including ones involved in the oxidative-stress response,
51 co-vary with viral transcriptional load. Overall, our work demonstrates remarkable heterogeneity in
52 the transcriptional outcome of influenza virus infection among nominally identical cells infected
53 with a relatively pure population of virions.

54 Results

55 Strategy to measure mRNA in single virus-infected cells.

56 We performed single-cell mRNA sequencing using a droplet-based system that physically isolates
57 individual cells prior to reverse transcription ([Zheng et al., 2017; Macosko et al., 2015; Klein et al., 2015](#)).
58 Each droplet contains primers with a unique *cell barcode* that tags all mRNAs from that
59 droplet during reverse-transcription. Each primer also contains a *unique molecular identifier (UMI)*
60 that is appended to each mRNA molecule during reverse transcription. The 3' ends of the mRNAs are
61 sequenced and mapped to the human and influenza virus transcriptomes to determine transcript
62 identities. This information is combined with that provided by the UMIs and cell barcodes to

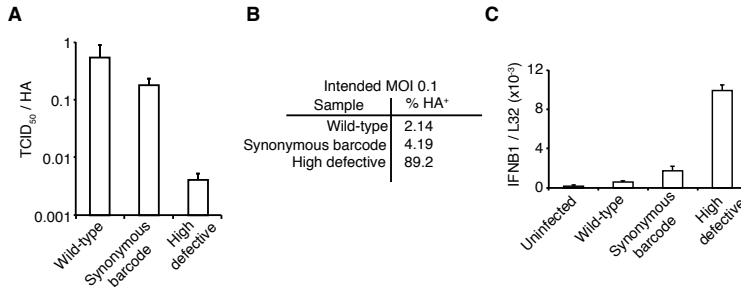


Figure 2. The viral stocks in our experiments are relatively pure of defective particles. **(A)** Our viral stocks have a higher ratio of infectious particles to HA virion RNA compared to a high-defective stock propagated at high MOI. HA viral RNA was quantified by qPCR on virions. Error bars \pm S.D., n=6 (qPCR replicates). **(B)** Our viral stocks have a higher ratio of infectious particles to particles capable of expressing HA protein. A549 cells were infected at an MOI of 0.1, and the percentage of cells expressing HA protein at 9 hours post-infection was quantified by antibody staining and flow cytometry. **(C)** Our viral stocks are less immunostimulatory than virus propagated at high MOI when used at the same number of infectious units as calculated by TCID50. Note that this fact does not necessarily imply that they are more immunostimulatory per virion, as the high-MOI stocks also have more virions per infectious unit as shown in the first two panels. Measurements of *IFNB1* transcript by qPCR normalized to the housekeeping gene L32 in A549 cells at 10 hours post infection at an MOI of 0.5. Error bars \pm S.D., n=3. Note that MOIs were calculated by TCID50 on MDCK-SIAT1 cells, whereas the experiments in this figure involved infection of A549 cells.

Figure 2-Figure supplement 1. Full flow cytometry data for panel B .

63 quantify the number of molecules of each mRNA species that have been captured for each cell.
 64 Infected cells will express viral as well as cellular mRNAs – however the cell barcodes and UMIs
 65 cannot distinguish whether a cell was initially infected by one or multiple viral particles. We therefore
 66 engineered an influenza virus (strain A/WSN/1933) that additionally carried *viral barcodes* consisting
 67 of synonymous mutations near the 3' end of each transcript (Figure 1A). Critically, these synonymous
 68 mutations did not greatly impact viral growth kinetics (Figure 1B). We infected A549 human lung
 69 carcinoma cells with an equal mix of the wild-type and synonymously barcoded viruses. Cells
 70 infected by a single virion will exclusively express mRNAs from either wild-type or synonymously
 71 barcoded virus, whereas cells that are co-infected with multiple virions will often express mRNAs
 72 from both the wild-type and synonymously barcoded viruses (Figure 1C).

73 We took care to generate stocks of virus that were relatively “pure” of defective particles. Stocks
 74 of viruses typically contain an array of biologically active viral particles, some of which are defective
 75 for replication owing to mutations or deletions in essential viral genes (*von Magnus, 1954; Huang*
et al., 1970; Brooke, 2014; Fonville et al., 2015; Lauring and Andino, 2010; Dimmock et al., 2014;
Saira et al., 2013). These defective particles become prevalent when a virus is grown at high MOI,
 76 where complementation permits the growth of otherwise deleterious genotypes. To minimize the
 77 levels of defective particles, we propagated our viral stocks at low MOI for a relatively brief period of
 78 time (*Xue et al., 2016*). We validated that our stocks exhibited greater purity of infectious particles
 79 than a stock propagated at high MOI by verifying that they had a higher ratio of infectious particles
 80 to virion RNA (Figure 2A) and to particles capable of inducing expression of a single viral protein
 81 (Figure 2B). In addition, viral stocks with many defective particles are more immunostimulatory
 82 per infectious unit (e.g., TCID50) than low-defective stocks (*Tapia et al., 2013; Lopez, 2014*), in part
 83 simply because there are more physical virions per infectious unit (Figure 2A,B). We confirmed that
 84 our viral stocks induced less interferon per infectious unit than a stock propagated at higher MOI
 85 (Figure 2C).

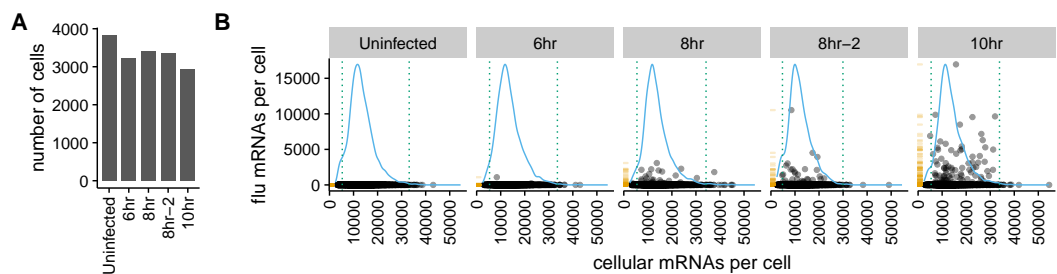


Figure 3. There is a very wide distribution in the amount of viral mRNA per cell. **(A)** Number of cells sequenced for each sample. **(B)** The number of cellular and viral mRNAs detected for each cell is plotted as a point. The blue lines show the overall distribution of the number of cellular mRNAs per cell. The orange rug plot at the left of each panel shows the distribution of the number of viral mRNAs per cell. Cells outside the dotted green lines were considered outliers with suspiciously low or high amounts of cellular mRNA (possibly derived from two cells per droplet), and were excluded from all subsequent analyses. Figure 3-Figure supplement 1 shows the exact distributions of the fraction of viral mRNA per cell.

Figure 3-Figure supplement 1. Cumulative fraction plot of proportion of total mRNA from virus.

88 **Single cells show an extremely wide range of expression of viral mRNA.**

89 We infected A549 cells at low MOI with a mixture of the wild-type and synonymously barcoded
90 viruses, and collected cells for sequencing at 6, 8, and 10 hours post-infection, including a replicate
91 a 8-hours. We replaced the infection inoculum with fresh media at one-hour post-infection, thereby
92 ensuring that most infection was initiated during a narrow time window. The exception was the
93 replicate 8-hour sample, for which we did *not* perform this media change and instead left the
94 cells in the original infection inoculum. We recovered between 3,000 and 4,000 cells for each
95 sample (Figure 3A). As expected for a low-MOI infection, most cells expressed little or no viral mRNA
96 (Figure 3B and Figure 3-Figure supplement 1). Also as expected, the amount of viral mRNA per cell
97 among infected cells increased over time (Figure 3B and Figure 3-Figure supplement 1). But what
98 was most notable was how widely the number of viral mRNA molecules varied among infected cells.
99 While the fraction of mRNA derived from virus was <0.1% for most cells, viral mRNA constituted
100 half the transcriptome in a few cells at 8 and 10 hours (Figure 3B).

101 A complicating factor is that uninfected cells could have small amounts of viral mRNA due
102 to leakage of transcripts from lysed cells. It is therefore important to establish a threshold for
103 identifying truly infected cells. We can do this by taking advantage of the fact that roughly half the
104 infecting virions bear synonymous barcodes. Reads derived from lysed cells will be drawn from
105 both wild-type and synonymously barcoded viral transcripts. However, most cells are infected by at
106 most one virion, and so the reads from truly infected cells will usually derive almost entirely from
107 one of the two viral variants. Figure 4A shows the fraction of viral reads in individual cells from each
108 viral variant, and Figure 4B indicates the fraction of viral reads from the most abundant variant in
109 that cell. Most cells with large amounts of viral mRNA have viral transcripts exclusively derived from
110 one viral variant – indicating non-random partitioning as expected from viral infection. However,
111 cells with a small amount of viral mRNA often have viral transcripts from both variants, as expected
112 from the random partitioning associated with simple mRNA leakage. Finally, a few cells with large
113 amounts of viral mRNA have viral transcripts from both variants, likely reflecting co-infection.

114 We determined the threshold amount of viral mRNA per cell for each sample at which the
115 barcode partitioning clearly resulted from infection rather than leakage (Figure 4C and Figure 4-
116 Figure supplement 2), and used these thresholds to annotate cells that we were confident were
117 truly infected. We also annotated as co-infected cells above this threshold that had mRNA from
118 both viral variants. Figure 4D shows the number of cells annotated as infected and co-infected for
119 each sample – these cells are just a small fraction of the number of cells with any viral read. These
120 annotation thresholds are conservative, and may miss some true low-level infections. However, it is
121 important that the analyses below are restricted to cells that are truly infected with virus, so we

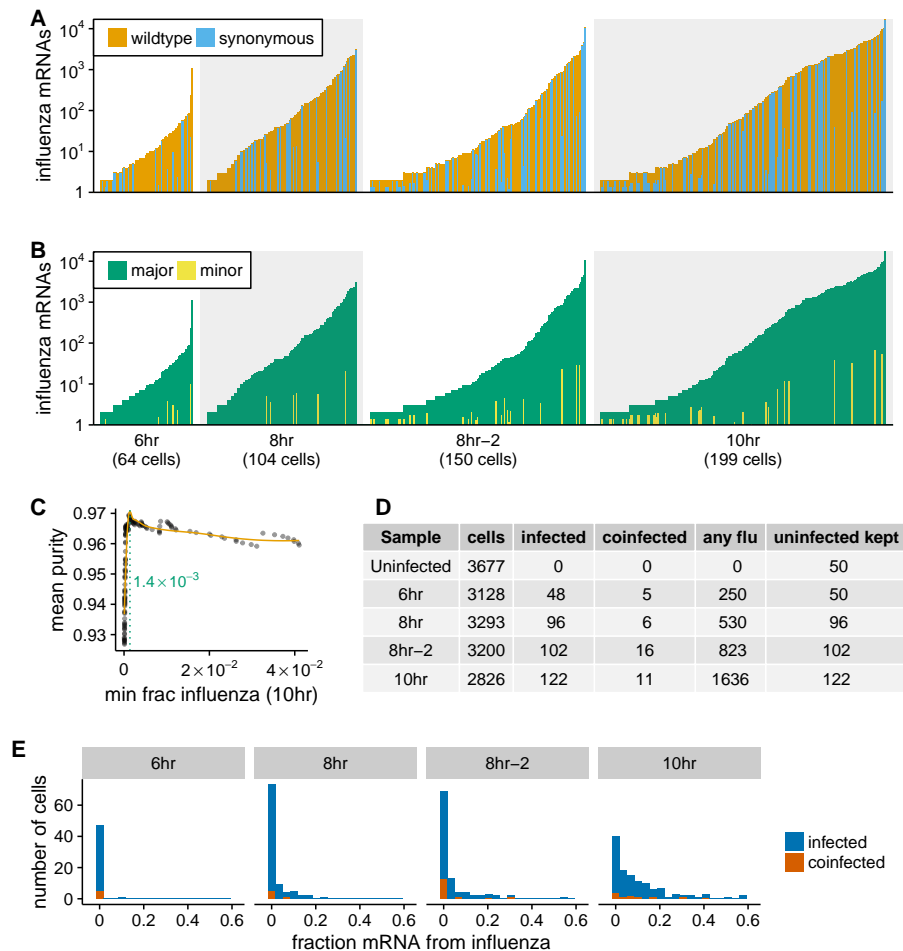


Figure 4. Synonymous barcodes on the viral mRNAs distinguish true infections from cells that contain viral mRNAs derived from leakage of lysed cells. **(A)** Cells with at least two viral mRNAs for which the barcode could be called, arranged in order of increasing influenza transcript counts. Bar heights denote the number viral mRNAs on a \log_{10} scale, bar coloring is linearly proportional to the fractions of viral mRNAs derived from wild-type and synonymously barcoded virus. **(B)** Same as (A), but each bar is colored according to the relative fraction of the more common (major) and less common (minor) virus variant. At low levels of viral mRNA there is often a roughly equal mix, suggesting contamination with viral mRNAs leaked from lysed cells. At higher levels of viral mRNA, cells generally have only one viral variant, suggesting infection initiated by a single virion. A few cells are also obviously co-infected with both viral variants. **(C)** We determined a threshold for calling “true” infections by finding the amount of viral mRNA per cell at which the viral barcode purity no longer increases with more viral mRNA. The purity is the fraction of all viral mRNA in a cell derived from the most abundant viral barcode in that cell. We fit a curve (orange line) to the mean purity of all cells with more than the indicated amount of viral mRNA, and drew the cutoff (dotted green line) at the point where this curve stopped increasing with the fraction of total mRNA derived from virus. This plot illustrates the process for the 10-hour sample, see Figure 4-Figure supplement 2 for similar plots for other samples. See the Methods for details. **(D)** The number of cells identified as infected and co-infected for each sample, as well as the number of cells with any viral read. For all subsequent analyses, we subsampled the number of uninfected cells per sample to the greater of 50 or the number of infected cells. **(E)** Distribution of the fraction of mRNA per cell derived from virus for both infected and co-infected cells.

Figure 4-Figure supplement 1. Number of viral barcodes called.

Figure 4-Figure supplement 2. Thresholds for calling infected cells.

Figure 4-Figure supplement 3. Fraction of total viral mRNA derived from a given fraction of infected cells.

Figure 4-Figure supplement 4. Flow cytometry analysis of viral protein production of cells contingent on infectious dose or coinfection state.

122 accepted the possible loss of some low-level infections in order to avoid false positives. In addition,
 123 the synonymous viral barcodes only identify co-infections by viruses with different barcodes – since
 124 the barcodes are at roughly equal proportion, we expect to miss about half of the co-infections.
 125 Since we annotate about ~10% of the infected cells as co-infected by viruses with different barcodes
 126 (Figure 4D), we expect another ~10% of the infected cells to also be co-infected but not annotated
 127 as so by our approach. Because most cells are not infected, we subsampled the uninfected cells to
 128 the numbers shown in Figure 4D to balance the proportions of infected and uninfected cells for all
 129 subsequent analyses.

130 Strikingly, the extreme variation in the number of viral transcripts per cell remains even after we
 131 apply these rigorous criteria for annotating infected cells (Figure 4E). The fraction of viral mRNA per
 132 infected cell follows a roughly exponential distribution, with many cells having few viral transcripts
 133 and a few cells having many. At 6 and 8 hours <10% of infected cells are responsible for over half
 134 the viral transcripts, while at 10 hours <15% of infected cells produce over half the viral transcripts
 135 (Figure 4-Figure supplement 3). Notably, Figure 4E shows that there are co-infected cells with both
 136 low and high amounts of viral mRNA, suggesting that the initial infectious dose does not drive a
 137 simple continuous increase in viral transcript production. In support of this view, we used flow
 138 cytometry to quantify the levels of individual viral proteins in cells infected at various MOIs or for
 139 which we could delineate co-infection status (Figure 4-Figure supplement 4). This analysis shows
 140 that sub-populations of cells that express similarly low and high levels of viral proteins persist
 141 across a wide range of infectious doses, although co-infection can influence the relative proportion
 142 of infected cells that fall into these sub-populations (Figure 4-Figure supplement 4).

143 **Absence of viral genes partially explains cell-to-cell variability in viral load.**

144 The influenza genome is segmented, and cells can fail to express a viral mRNA if the encoding
 145 gene segment is not packaged in the infecting virion or fails to initiate transcription after infection.
 146 Indeed, several groups have reported that the majority of infected cells fail to express at least
 147 one viral gene (*Brooke et al., 2013; Heldt et al., 2015; Dou et al., 2017*). We wondered if the
 148 absence of specific viral genes might be associated with reduced amounts of viral mRNA within
 149 single infected cells. In particular, transcription of influenza virus mRNAs is performed by the viral
 150 ribonucleoprotein (RNP) complex, which consists of the three proteins that encode the tripartite
 151 polymerase (PB2, PB1, and PA) as well as nucleoprotein (NP) (*Huang et al., 1990*). Each viral gene
 152 segment is associated with one RNP in incoming infecting virions, but secondary transcription by
 153 newly synthesized RNPs requires the presence of the viral genes encoding each of the four RNP
 154 proteins (*Vreede et al., 2004; Eisfeld et al., 2015*). This secondary transcription is a major source
 155 of viral mRNAs, as evidenced by the fact that blocking synthesis of the RNP proteins reduces the
 156 amount of viral mRNA by several orders of magnitude in bulk cells (Figure 5-Figure supplement 1).

157 We examined the total amount of viral mRNA versus the expression of the genes from each viral
 158 segment (Figure 5A, Figure 5-Figure supplement 2). Note that influenza virus expresses ten major
 159 gene transcripts from its eight gene segments, as the M and NS segments are alternatively spliced
 160 to produce the M1 / M2 and NS1 / NEP transcript, respectively (*Dubois et al., 2014*). However, an
 161 inherent limitation of current established single-cell mRNA sequencing techniques is that they only
 162 sequence the 3' end of the transcript (*Zheng et al., 2017; Macosko et al., 2015; Klein et al., 2015*;
 163 *Cao et al., 2017*). Since the alternative spliceforms M1 / M2 and NS1 / NEP share the same 3' ends,
 164 we cannot distinguish them and therefore will refer simply to the combined counts of transcripts
 165 from each of these alternatively spliced segments as the M and NS genes.

166 Cells that lack an RNP gene never derive more than a few percent of their mRNAs from virus,
 167 confirming the expected result that all four RNP genes are essential for high levels of viral transcrip-
 168 tion (Figure 5A, Figure 5-Figure supplement 2). However, we observe cells that lack each of the other
 169 non-RNP genes but still derive ≈40% of their mRNAs from virus, suggesting that none of the other
 170 genes are important for high levels of viral transcription. These results are statistically supported by
 171 Figure 5B, which shows that absence of any RNP gene but *not* any other viral gene is associated

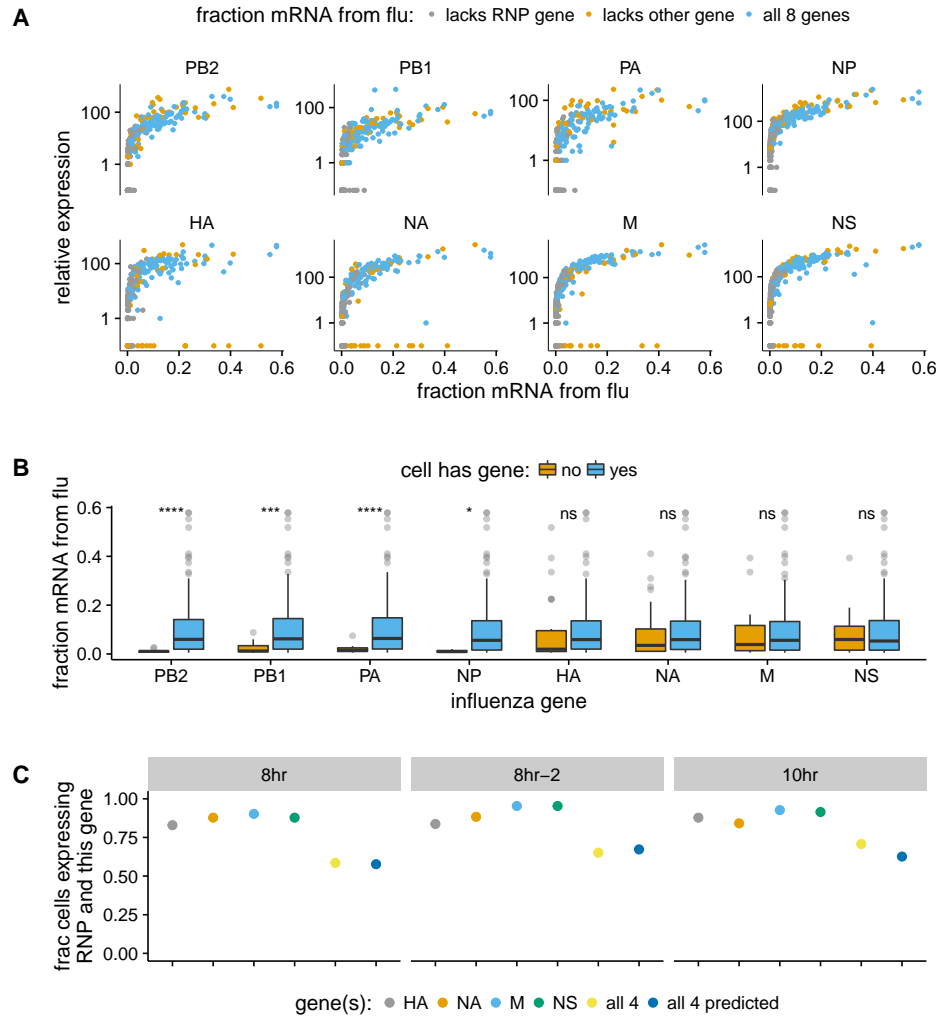


Figure 5. The absence of viral genes explains some of the variability in the amount of viral mRNA per cell. **(A)** The normalized expression of each viral gene as a function of the total fraction of mRNA in each infected cell derived from virus, taken over all time points. Cells with high viral burden always express all RNP genes, but some cells with high viral burden lack each of the other genes. **(B)** Box and whisker plots showing the per-cell viral burden among cells with >0.5% of their mRNA from virus, binned by whether or not the cells express each gene. A Wilcoxon signed-rank test was used to test the null hypothesis that absence of each gene does not affect viral burden: **** = $P < 10^{-4}$, *** = $P < 10^{-3}$, * = $P < 0.05$, ns = not significant. **(C)** The fraction of cells that express each of the four other genes among cells that express all RNP genes, as well as the fraction that express *all* four of the other genes. The fraction that express *all* four genes is well predicted by simply multiplying the frequencies of cells that express each gene individually, indicating that gene absence is approximately independent across these genes.

Figure 5-Figure supplement 1. Secondary transcription is a major source of viral mRNA during bulk infections.

Figure 5-Figure supplement 2. Like panel (A), but shows samples individually.

Figure 5-Figure supplement 3. Like panel (B) but for the 10-hr sample only.

Figure 5-source data 1. The numerical data for panel (C) are in p_missing_genes.csv.

172 with reduced amounts of viral mRNA. However, gene absence clearly does not explain all of the
 173 variability in viral gene expression, since even cells expressing all viral genes exhibit a very wide
 174 distribution in the amount of viral mRNA that they express. Specifically, at both 8 and 10 hours, the
 175 amount of viral mRNA in individual cells expressing all eight viral genes still ranges from <1% to
 176 >50% (Figure 5A, Figure 5-Figure supplement 2).

177 We also quantified the fraction of infected cells that completely failed to express a given gene. We
 178 limited this analysis to examining the presence / absence of the non-RNP genes in cells expressing
 179 all four RNP genes, since we might fail to detect viral transcripts that are actually present at low
 180 levels in RNP-deficient cells due to the lower viral burden in these cells. At the 8- and 10-hour time
 181 points, between 5% and 17% of cells fail to express any one of the four non-RNP genes (Figure 5C
 182 and Figure 5-source data 1). The absence of a given gene appears to be an independent event, as
 183 the probability of observing all four non-RNP genes in a cell is well predicted by simply multiplying
 184 the probabilities of observing each gene individually (Figure 5C and Figure 5-source data 1). If we
 185 extrapolate the frequencies at which cells lack non-RNP genes to the RNP genes, then we would
 186 predict that 35-50% of infected cells express mRNAs from all eight genes. This estimate of the
 187 frequency at which infected cells express mRNAs from all eight gene segments is slightly higher than
 188 previous estimates of 13% (*Brooke et al., 2013*) and 20% (*Dou et al., 2017*). At least one difference
 189 is that *Brooke et al. (2013)* stained for proteins whereas we examined the expression of mRNAs – it
 190 is likely that some cells contain mutated viral genes that fail to produce stable protein even when
 191 mRNA is expressed.

192 **The relative amounts of different viral mRNAs are more consistent across cells.**

193 The results above show that the amount of viral mRNA in infected cells varies over several orders
 194 of magnitude. Does the relative expression of viral genes exhibit similar cell-to-cell variability?
 195 To address this question, we focused on cells that derived >5% of their mRNA from virus, since
 196 estimates of relative viral gene expression will be less noisy in cells with more viral mRNAs.

197 In contrast to the extreme variability in the total viral mRNA per cell, the fraction of this mRNA
 198 derived from each gene is much more consistent across cells (Figure 6A). Total viral mRNA varies by
 199 orders of magnitude, but the fraction from any given viral gene is fairly tightly clustered around the
 200 median value for all cells (Figure 6B). The relative levels of each viral mRNA in our cells are similar
 201 to prior bulk measurements made by Northern blots (*Hatada et al., 1989*), which also found an
 202 expression hierarchy of M > NS > NP > NA > HA > PB2 ~ PB1 ~ PA. The cell-to-cell consistency in
 203 the relative expression of different viral genes is even tighter if we limit the analysis only to cells
 204 that express all eight viral genes (Figure 6C,D). Therefore, with the exception of complete gene
 205 absence, the factors that drive the dramatic cell-to-cell variability in the amount of viral mRNA have
 206 roughly similar effects on all viral genes in a given cell. This finding is consistent with prior work
 207 showing positive correlations among the abundance of several viral genome segments in individual
 208 cells (*Heldt et al., 2015*).

209 **Co-infection can provide infected cells with the full complement of viral genes.**

210 Our sequencing enables us to identify the rare cells that were co-infected with both wild-type and
 211 synonymously barcoded viral variants. Overall, we captured 10 such co-infected cells that had >5%
 212 of their mRNA derived from virus (Figure 7). Seven of these 10 cells expressed all eight viral genes.
 213 The majority (4 of 7) of these cells would *not* have expressed all the viral genes in the absence
 214 of co-infection, since they have at least one gene exclusively derived from each viral variant. For
 215 instance, the cell with 11.2% of its mRNA from virus in the upper right of Figure 7 expresses M only
 216 from the wildtype viral variant, and NP and HA only from the synonymously barcoded variant. Our
 217 data therefore provide the first direct single-cell observation of the fact that co-infection can rescue
 218 missing viral genes (*Brooke et al., 2013, 2014; Fonville et al., 2015; Aguilera et al., 2017*).

219 Another observation from Figure 7 is that co-infected cells usually express roughly equal
 220 amounts of transcripts from each of the two viral variants. This observation is consistent with the
 221 finding by *Dou et al. (2017)* and *Huang et al. (2008)* that the temporal window for co-infection is
 222 short – if both viral variants infect a cell at about the same time, then neither will have a headstart
 223 and so each will have a roughly equal opportunity to transcribe its genes.

224 To support this idea with a larger dataset albeit at lower resolution, we generated a virus
 225 in which the HA coding sequence was replaced by GFP. We then co-infected cells with a mix of

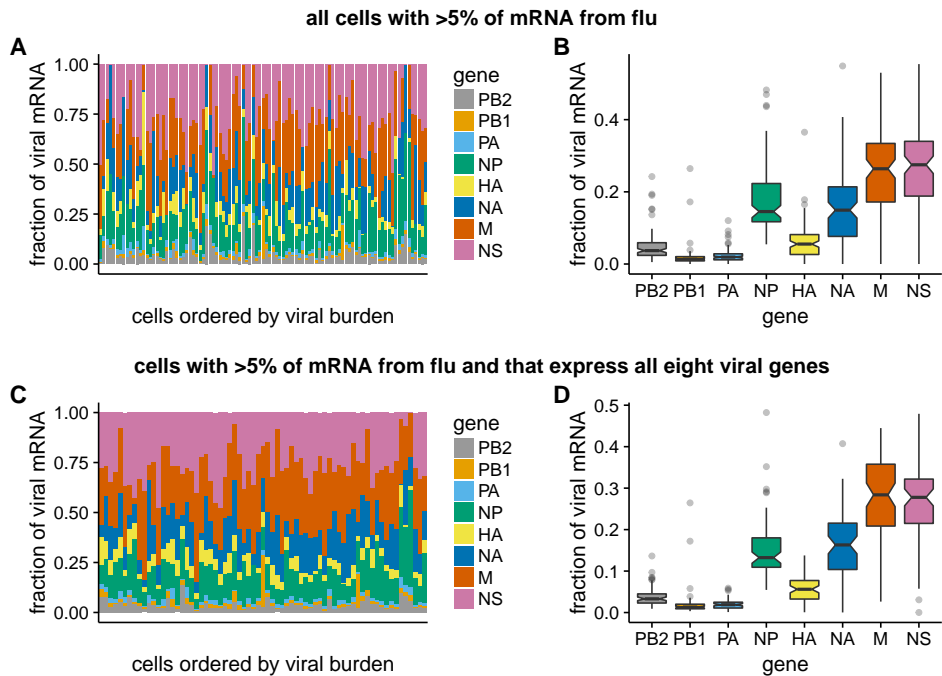


Figure 6. [add expression wedges] Relative expression of influenza virus genes in highly infected cells (>5% of total mRNA from virus). **(A)** The fraction of viral mRNA from each viral gene for each cell. **(B)** Box plots showing the distribution of the fraction of viral mRNA per cell from each viral gene. The black lines at the notches are the medians, and the tops and bottoms of boxes indicate the first and third quartiles. Whiskers extend to the highest or lowest data point observed within 1.5x the interquartile range, outliers shown as circles. Notches extend 1.58x the interquartile range divided by the square root of the number of observations. **(C), (D)** The same plots, but only including cells for which we observed at least one molecule of each viral gene.

Figure 6-source data 1. The raw data for all cells are in `p_flu_expr_all.csv`.

Figure 6-source data 2. The raw data for fully infected cells are in `p_flu_expr_fullyinfected.csv`.

wildtype and Δ HA-GFP virus and used flow cytometry to score cells for the presence of HA only (infection by wildtype virus), GFP only (infection by Δ HA-GFP virus), or both (co-infection) as shown in Figure 7 Figure supplement 1. As in our single-cell sequencing data, we found that expression of HA and GFP were highly correlated, indicating that co-infected cells typically expressed roughly equal amounts of transcript from each viral variant.

Activation of the interferon response is rare in single infected cells.

Because our sequencing captured all polyadenylated transcripts, we can examine whether there are prominent changes in the host-cell transcriptome in sub-populations of infected cells. Influenza virus infection can trigger innate-immune sensors that lead to the transcriptional induction of type I and III interferons, and subsequently of anti-viral interferon-stimulated genes (*Killip et al., 2015; Iwasaki and Pillai, 2014; Crotta et al., 2013*). However, activation of the interferon response is stochastic and bi-modal at the level of single cells (*Chen et al., 2010; Shalek et al., 2013, 2014; Perez-Cidoncha et al., 2014; Bhushal et al., 2017; Hagai et al., 2017*). We therefore hypothesized that we might see two sub-populations of infected cells: one in which the interferon response inhibited viral transcription, and another in which the virus was able to express high levels of its mRNA by evading or blocking this response.

To examine whether there were distinct sub-populations of virus-infected cells, we used a semi-supervised t-SNE approach (*Van der Maaten and Hinton, 2008*) to cluster cells by genes that co-varied with viral infection status. As shown in Figure 8A,B, this approach effectively grouped cells by the amount of viral mRNA that they expressed. Sample-to-sample variation was regressed away

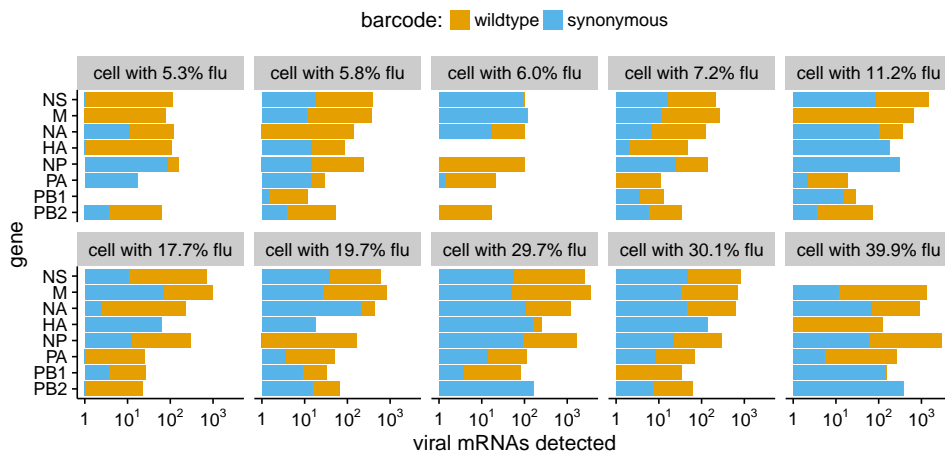


Figure 7. The abundance of each viral transcript in cells that are co-infected with the two viral variants and have >5% of their mRNA derived from virus. The bars show the logarithms of the numbers of each viral mRNA detected, and are colored in linear proportion to the fraction of that mRNAs derived from wild-type or synonymously barcoded virus.

Figure 7-Figure supplement 1. Co-infected cells express roughly equal amounts of a gene from each infecting viral variant.

Figure 7-source data 1. The raw data plotted in this figure are in `p_co-infection.csv`.

Figure 7-source data 2. The sequence of the HA viral RNA carrying the GFP gene is in `HAflank-eGFP.fasta`.

246 during the clustering, as cells did not obviously group by time-point, with expected exception that
247 the uninfected and 6-hour samples had few cells in the region of the plot corresponding to large
248 amounts of viral mRNA (Figure 8C).

249 But to our surprise, we did not see a prominent clustering of infected cells into sub-populations
250 as expected if the interferon response was strongly activated in some cells. To investigate fur-
251 ther, we annotated each cell by the total number of type I and III interferon transcripts detected.
252 Remarkably, only a single cell expressed detectable interferon (Figure 8D). We also examined
253 interferon-stimulated genes, which are induced by autocrine and paracrine interferon signaling.
254 Figure 8E shows expression of one such gene, IFIT1 (*Fensterl and Sen, 2011*). As with interferon
255 itself, expression of IFIT1 was rare and most prominent in the single interferon-positive cell, pre-
256 sumably due to the higher efficiency of autocrine versus paracrine signaling. Notably, interferon
257 and interferon-stimulated genes were also relatively ineffective at blocking viral transcription in the
258 single cell in which they were potently induced, since >10% of the mRNA in this cell was derived
259 from virus (Figure 8A,B,D,E).

260 We posited that the paucity of interferon induction might be due to the activity of influenza
261 virus's major interferon antagonist, the NS1 protein (*García-Sastre et al., 1998; Hale et al., 2008*).
262 We therefore identified cells that expressed substantial amounts of viral mRNA but lacked the
263 NS gene (Figure 8F). Consistent with the idea that NS1 is important for suppressing interferon,
264 the one interferon-positive cell lacked detectable expression of the NS gene. But other cells that
265 lacked NS expression still failed to induce a detectable interferon response, despite often having a
266 substantial amount of their mRNA derived from virus (Figure 8). This result is in line with other work
267 showing that NS1-deficient influenza virus does not deterministically induce interferon (*Killip et al.,
268 2017; Kallfass et al., 2013*). Therefore, many individual infected cells fail to activate innate-immune
269 responses even when the virus lacks its major interferon antagonist.

270 **Some host genes co-vary with viral gene expression.**

271 We examined whether any host genes were differentially expressed in cells with more viral mRNA.
272 We restricted this analysis to infected cells with all eight viral genes in order to focus on cellular

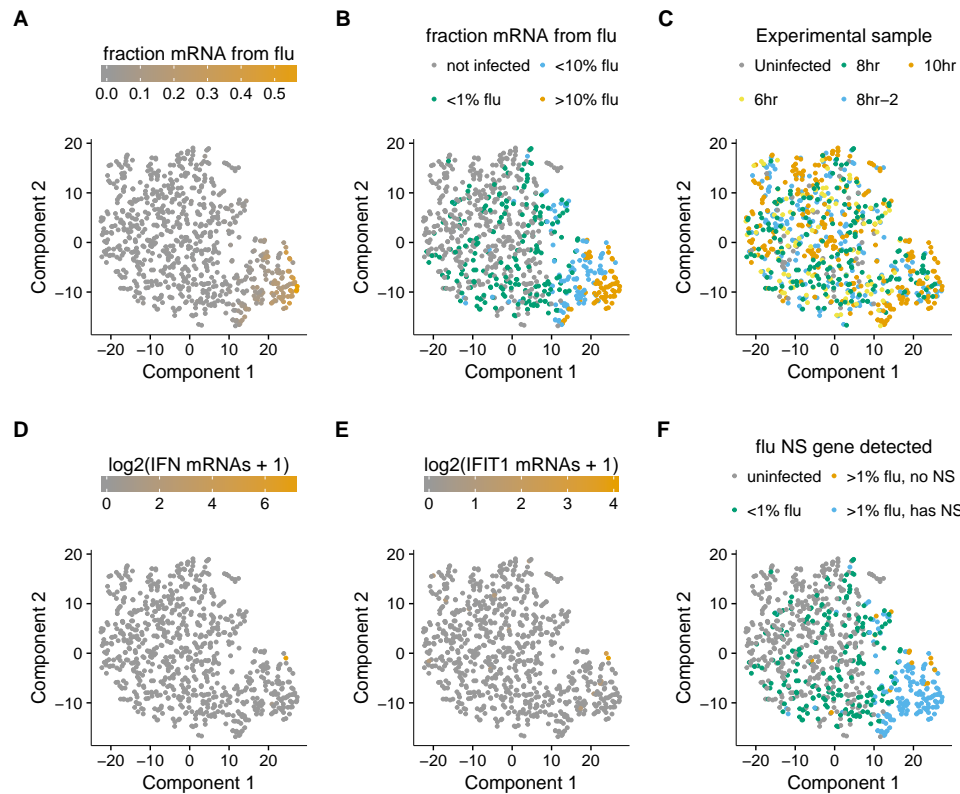


Figure 8. [add arrow] A t-SNE plot created by semi-supervised clustering using genes that co-vary with viral infection status. Each point is a single cell, and each panel shows an identical layout but colors the cells according to a different property. **(A), (B)** Cells colored by the fraction of their mRNA derived from virus. **(C)** Cells colored by the experimental sample. **(D), (E)** Cells colored by the number of detected transcripts from type I and III interferons (IFN). Only one cell has detectable interferon expression (in orange, indicated with arrow). **(E)** Cells colored by the expression of the interferon-stimulated gene IFIT1. **(F)** Cells colored by whether they express the viral NS gene. The one interferon-positive cell is lacking NS, but so are many interferon-negative cells.

genes that were associated with viral mRNA burden independent of effects due to the presence or absence of particular viral transcripts. We identified 43 cellular genes that co-varied with viral gene expression at a false discovery rate of 0.1 (Figure 9).

Many of the genes with increased expression in cells with more viral mRNA are known or suspected to be regulated by the Nrf2 master regulator in response to oxidative stress. These genes produce proteins that are involved in detoxification of reactive oxygen species or resultant products, the management of misfolded proteins, the electron transport chain, or a general stress response (Figure 9—Figure supplement 1). We additionally see reduced expression of the nitric oxide synthase interacting protein (NOSIP). Transient oxidative stress is known to occur during viral infection, and may act in a proviral fashion via MAPK activation driving vRNP export (Amatore et al., 2014). The antioxidant response is thought to be largely antiviral, potentially through inhibition of MAPK activity (Lin et al., 2016; Sgarbanti et al., 2014). Our data do not reveal whether the expression of genes involved in the response to oxidative stress are a cause or a symptom of higher levels of viral mRNA, and further investigation of this topic is an interesting area for future work.

Discussion

We have quantified the total transcriptome composition of single cells infected with influenza virus. While we observe a general increase in the amount of viral mRNA over time as expected from

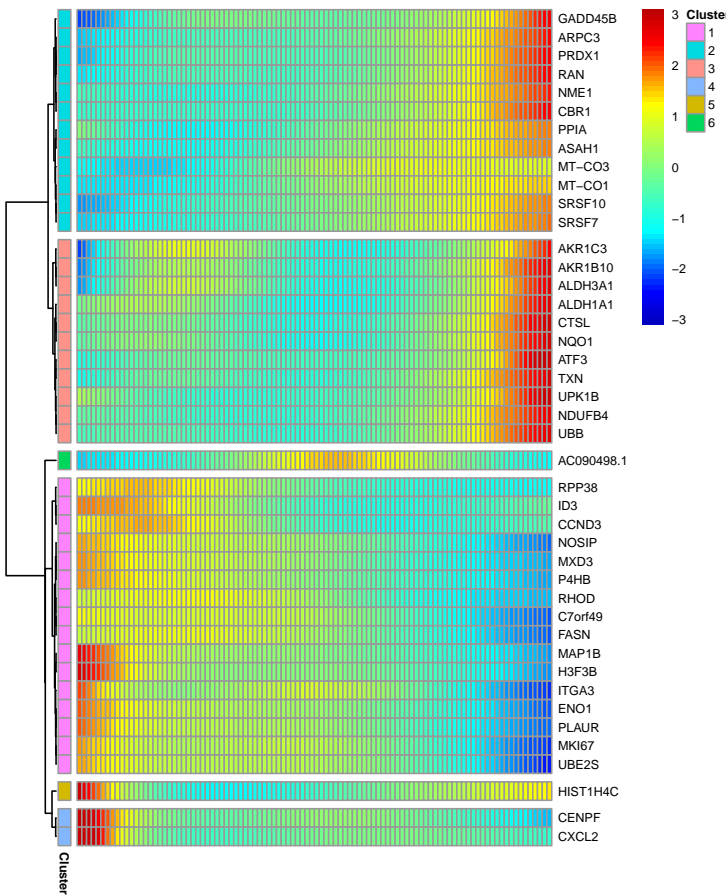


Figure 9. [add gray arrow wedge] Cellular genes that co-vary in expression with the amount of viral mRNA in cells expressing all eight viral genes. The columns are cells, ordered from left to right by the fraction of mRNA derived from virus. Each row is a gene that is differentially expressed as a function of the fraction of mRNA derived from virus at a false discovery rate of 0.1. Genes for which the color goes from blue at left to red at right are expressed at higher levels in cells with more viral mRNA. The scale bar indicates the number of standard deviations above or below the mean expression, truncated at 3-fold on both sides.

Figure 9-source data 1. The full results of the differential expression test is in `p_sig_cellular_genes.csv`.

Figure 9-source data 2. The results of a gene-set analysis are in `p_pathway_enrichment.tsv`.

Figure 9-Figure supplement 1. Many genes that co-vary with viral load are involved in the oxidative stress response.

290 bulk measurements (*Hatada et al., 1989; Shapiro et al., 1987*), there is wide variation in viral gene
291 expression among individual infected cells.

292 The most obvious form of heterogeneity is the complete failure of some infected cells to express
293 one or more viral genes, which we estimate occurs in about half the infected cells in our experiments.
294 The absence of some viral genes in some infected cells has been noted previously (*Brooke et al.,
295 2013; Heldt et al., 2015; Dou et al., 2017*), and our work provides a holistic view by quantifying the
296 total viral transcriptional load as a function of the level of each mRNA. We find that cells lacking
297 expression of any of the four genes that encode the viral RNP express much less total viral mRNA,
298 consistent with prior bulk studies (*Vreeede et al., 2004; Eisfeld et al., 2015*). Interestingly, the reason
299 some cells fail to express some viral genes remains unclear. The prototypical influenza virion
300 packages one copy of each of the eight gene segments (*Noda et al., 2006; Hutchinson et al., 2010*),
301 but some virions surely package fewer (*Brooke et al., 2014*). However, it is also possible that much
302 of the viral gene absence is due to stochastic loss of viral RNPs after infection but prior to the
303 initiation of viral transcription in the nucleus.

304 The absence of viral genes only partially explains the cell-to-cell variation in amount of viral
 305 mRNA, which still varies from <1% to >50% among cells expressing all the viral genes. It is likely
 306 that other viral genetic factors explain some of this remaining heterogeneity. The 3'-end sequencing
 307 strategy used in our experiments detects the presence of a viral gene, but does not identify
 308 whether that gene contains a mutation that might hinder viral replication. However, viral mutations
 309 are also unlikely to explain all the observed heterogeneity, since current consensus estimates of
 310 influenza virus's mutation rate suggest that the typical virion in a stock such as the one used in our
 311 experiment should contain less than one mutation per genome (*Parvin et al., 1986; Suárez et al.,*
 312 *1992; Suárez-López and Ortín, 1994; Nobusawa and Sato, 2006; Bloom, 2014; Pauly et al., 2017*).

313 The rest of the heterogeneity must be due to some combination of cellular factors and inherent
 314 stochasticity. Some features of the cellular transcriptome co-vary with the amount of influenza
 315 mRNA. In particular, the viral load in individual cells is associated with the expression of genes
 316 involved in response to cellular stresses, including oxidative stress. It will be interesting to determine
 317 if these cellular transcriptional signatures are simply a consequence of the stress imposed by viral
 318 replication, or if their stronger activation in some cells is a causative factor that promotes viral
 319 transcription. However, it also would not be surprising if a substantial amount of the cell-to-cell
 320 heterogeneity cannot be ascribed to pre-existing features of either the viral genome or cellular state.
 321 Apparently stochastic heterogeneity is a common feature of many processes at a single-cell level (*Cai*
 322 *et al., 2006; Raj et al., 2006; Buganim et al., 2012; Shalek et al., 2013; Avraham et al., 2015*) –
 323 especially when those processes are initiated by very small numbers of initial molecules (*Elowitz*
 324 *et al., 2002*), as is the case for low-MOI viral infection.

325 Our data do suggest that the factors driving the heterogeneity in viral transcriptional load exert
 326 relatively concordant effects on all viral genes in a given cell. Specifically, despite the extreme
 327 heterogeneity in total viral mRNA per cell, the relative levels of the viral mRNAs are reasonably
 328 consistent across cells, and generally reflective of classical bulk measurements (*Hatada et al., 1989*).
 329 Therefore, despite the stochasticity inherent in initiating transcription and replication of each gene
 330 from a single copy carried by the incoming virion, as long as a gene is not completely lost then the
 331 virus possesses mechanisms to control its relative expression (*Shapiro et al., 1987; Hatada et al.,*
 332 *1989; Perez et al., 2010; Heldt et al., 2012; Chua et al., 2013*).

333 One factor that surprisingly does *not* appreciably contribute to the heterogeneity in our ex-
 334 periments is activation of innate-immune interferon pathways. Only one of the hundreds of
 335 virus-infected cells expresses any detectable interferon, despite the fact that a number of cells fail
 336 to express the influenza-virus interferon antagonist NS1. It is known that interferon activation is
 337 stochastic at the level of single cells in response to both synthetic ligands (*Shalek et al., 2013, 2014;*
 338 *Bhushal et al., 2017; Hagai et al., 2017*) and actual infection (*Rand et al., 2012; Perez-Cidoncha*
 339 *et al., 2014; Avraham et al., 2015; Killip et al., 2017*). But interferon expression is a prominent
 340 transcriptional signature of high-MOI influenza virus infection of bulk cells, including in the epithelial
 341 cell line and at the time-points used in our experiments (*Geiss et al., 2002; Sutejo et al., 2012*). So
 342 it is notable how rarely single cells express interferon. Interferon expression would surely be more
 343 common at later times or with a viral stock passaged at higher MOI, since paracrine interferon
 344 signaling (*Crotta et al., 2013*) and accumulation of defective viral particles enhance innate-immune
 345 detection (*Tapia et al., 2013; Lopez, 2014*). However, the early events of physiological influenza
 346 infection involve just a few virions (*Varble et al., 2014; McCrone et al., 2017*), and so it is interesting
 347 to speculate whether rare events such as interferon activation during the first few cycles of viral
 348 replication could contribute to heterogeneity in the eventual outcome of infection.

349 Overall, our work shows the power and importance of characterizing cellular infection at the
 350 level of single cells (*Avraham et al., 2015*). The dynamics of viral infection in any given cell is shaped
 351 by the genetic composition of the incoming virion, the host-cell state, the bi-modality of innate-
 352 immune activation, and the inherent stochasticity of molecular processes initiated by a single copy
 353 of each viral gene. We have shown how the confluence of these factors leads to extreme cell-to-cell
 354 heterogeneity in the transcriptional outcome of influenza virus infection. Further deconstruction of

355 the contributions of each factor will enable a deeper understanding of how the bulk features of
 356 infection emerge from the processes occurring within individual virus-infected cells.

357 Methods and Materials

358 Cell lines and viruses

359 The following cell lines were used in this study: the human lung epithelial carcinoma line A549
 360 (ATCC CCL-185), the MDCK-SIAT1 variant of the Madin Darby canine kidney cell line overexpressing
 361 human SIAT1 (Sigma-Aldrich 05071502), and the human embryonic kidney cell line 293T (ATCC
 362 CRL-3216). All cells were maintained in D10 media (DMEM supplemented with 10% heat-inactivated
 363 fetal bovine serum, 2 mM L-glutamine, 100 U of penicillin/ml, and 100 µg of streptomycin/ml) at 37
 364 °C at 5 % CO₂.

365 Wildtype A/WSN/1933 (H1N1) influenza virus was generated by reverse genetics using the
 366 plasmids pHW181-PB2, pHW182-PB1, pHW183-PA, pHW184-HA, pHW185-NP, pHW186-NA, pHW187-
 367 M, and pHW188-NS (*Hoffmann et al., 2000*). The sequences of the viral RNAs encoded in these
 368 plasmids are in Figure 1-source data 1. Reverse-genetics plasmids encoding the synonymously
 369 barcoded WSN virus were created by using site-directed mutagenesis to introduce two synonymous
 370 mutations near the 3' end of the mRNA for each viral gene. The sequences of the synonymously
 371 barcoded viral RNAs are in Figure 1-source data 1.

372 To generate viruses from these plasmids, we transfected an equimolar mix of all eight plasmids
 373 into cocultures of 293T and MDCK-SIAT1 cells seeded at a ratio of 8:1. At 24 hours post-transfection,
 374 we changed media from D10 to influenza growth media (Opti-MEM supplemented with 0.01% heat-
 375 inactivated FBS, 0.3% BSA, 100 U of penicillin/ml, 100 µg of streptomycin/ml, and 100 µg of calcium
 376 chloride/ml). At 48 hours post-transfection we harvested the virus-containing supernatant, pelleted
 377 cellular material by centrifugation at 300 x g's for 4 minutes, and stored aliquots of the clarified
 378 viral supernatant at -80 °C. We then titered thawed aliquots of viral by TCID50 on MDCK-SIAT1 cells,
 379 computing titers via the formula of *Reed and Muench (1938)*. To generate our "high-purity" stocks of
 380 viruses for the single-cell sequencing experiments, we then infected MDCK-SIAT1 cells at an MOI of
 381 0.01, and let the virus replicate for 36 hours prior to harvesting aliquots that were again clarified by
 382 low-speed centrifugation, aliquoted, stored at -80 °C, and titered by TCID50. The high-MOI passage
 383 (high-defective particle) stock used in Figure 2 was generated by instead passaging in MDCK-SIAT1
 384 cells twice at an MOI of 1 for 48 hours.

385 For the experiments in Figure 7-Figure supplement 1, we created a virus that carried an HA gene
 386 segment in which GFP replaced most of the HA coding sequence, following a scheme first described
 387 by *Marsh et al. (2007)*. Briefly, we created a plasmid encoding a viral RNA with GFP in place of the
 388 HA coding sequence in the context of the pH21 (*Neumann et al., 1999*) reverse-genetics plasmid,
 389 removing potential start codons upstream of the GFP (see Figure 7-source data 2 for the sequence
 390 of the viral RNA). We then generated GFP-carrying virus by reverse-genetics in cells constitutively
 391 expressing HA (*Doud and Bloom, 2016*). To obtain sufficient titers, this HA-eGFP virus was expanded
 392 for 44 rather than 36 hours after initiating infection at an MOI of 0.01.

393 qPCR

394 For the qPCR in Figure 2 and Figure 5-Figure supplement 1, A549 cells were seeded at 3x10⁵
 395 cells per well in a 6-well tissue culture plate in D10 the day prior to infection. On the day of
 396 infection, a single well was trypsinized and the cells were counted in order to determine the
 397 appropriate amount of virus to use to achieve the intended MOI. Immediately before infection,
 398 D10 was replaced with influenza growth media. For cells incubated with cyclohexamide, the
 399 compound was added to a final concentration of 50 µg/ml at the time of infection – previously
 400 confirmed to be sufficient to halt viral protein production (*Killip et al., 2014*). RNA was purified
 401 using the QIAGEN RNeasy plus mini kit following manufacturer's instructions. cDNA was syn-
 402 thesized using an oligoDT primer and the SuperScript™ III first-strand synthesis supermix from

403 ThermoFisher using the manufacturer's protocol. Transcript abundance was measured using
 404 SYBR™ green PCR master mix, using a combined anneal/extension step of 60 °C for one minute
 405 with the following primers: *HA*: 5'-GGCCCAACCACACATTCAAC-3', 5'-GCTCATCACTGCTAGACGGG-
 406 3', *IFNB1*: 5'-AAACTCATGAGCAGTCTGCA-3', 5'-AGGAGATCTTCAGTTCGGAGG-3', *L32*: 5'-
 407 AGCTCCCCAAAATAGACGCAC-3', 5'-TTCATAGCAGTAGGCACAAAGG-3'. Biological triplicates were per-
 408 formed for all samples.

409 For the measurements of viral genomic HA content in Figure 2A, vRNA was harvested from 80
 410 µl of viral supernatant by the addition of 600 µl of RLT plus before proceeding with the standard
 411 QIAGEN RNeasy Plus Mini kit protocol. The cDNA was generated using SuperScript™ III first-strand
 412 synthesis supermix using the manufacturer's protocol, and using the universal vRNA primers of
 413 **Hoffmann et al. (2001)** with the modifications described in **Xue et al. (2017)**. The qPCR was then
 414 performed as for mRNA measurements. A standard curve was generated from three independent
 415 dilutions of the HA-encoding reverse genetics plasmid. All vRNA values represent three independent
 416 RNA extractions with two replicate qPCR measurements.

417 **Flow cytometry titering and analyses**

418 To determine viral titers in terms of HA-expressing units and for the flow cytometry in Figure 7,
 419 Figure supplement 1, and Figure supplement 4 A549 cells were seeded in a 6-well plate and infected
 420 as described above for the qPCR analyses. Cells were harvested by trypsinization, resuspended in
 421 phosphate-buffered saline supplemented with 2% heat-inactivated FBS, and stained with 10 µg/ml
 422 of H17-L19, a mouse monoclonal antibody confirmed to bind to WSN HA in a prior study (**Doud**
 423 **et al., 2017**). After washing in PBS supplemented with 2% FBS, the cells were stained with a goat
 424 anti-mouse IgG antibody conjugated to APC. Cells were then washed, fixed in 1% formaldehyde,
 425 and washed further before a final resuspension and analysis. We then determined the fraction of
 426 cells that were HA positive and calculated the HA-expressing units. For NS1 staining in Figure sup-
 427 plement 4, cells stained for HA as described above were permeabilized using BD Cytofix/Cytoperm
 428 following manufacturer's instructions, stained with anti-NS1 (GTX125990, Genetex) at 4.4 µg/ml,
 429 washed, stained with a goat anti-rabbit IgG antibody conjugated to Alexa Fluor 405. washed, and
 430 analyzed. For Figure 7, Figure supplement 1, and Figure supplement 4), after gating to exclude
 431 multiplets in FlowJo, data were extracted using the R package flowCore (**Le Meur et al., 2007**) and
 432 analyzed using a custom Python script. For Figure supplement 4) channels were additionally com-
 433 pensated in FlowJo. Guassian kernel density estimates were obtained using the scipy stats package
 434 method, guassian_kde, using automatic bandwidth determination (**van der Walt et al., 2017**). For
 435 Figure supplement 4), the percentage of influenza-infected cells was determined by HA staining
 436 alone, and the top quantile of NS1-stained cells matching that percentage were taken as the NS1
 437 positive population.

438 **Infections for single-cell mRNA sequencing**

439 Single-cell sequencing libraries were generated using the 10x Chromium Single Cell 3' plat-
 440 form (**Zheng et al., 2017**) using the V1 reagents.

441 All time points except for the 8-hour replicate were prepared on the same day. For the infections,
 442 A549 cells were seeded in a 6-well plate, with two wells per time point. A single well of cells was
 443 trypsinized and counted prior to initiation of the experiment for the purposes of calculating MOI.
 444 Wild-type and synonymously barcoded virus were mixed to an estimated ratio of 1:1 based on prior,
 445 exploratory, single-cell analyses (data not shown). At the initiation of our experiment, the wells
 446 for all time points were changed from D10 to influenza growth media. Cells were then infected
 447 with 0.3 HA-expressing units of virus per cell (a determined by flow cytometry). The infections
 448 were performed in order of time point: first the 10-hour time point, then the 8-hour, and then the
 449 6-hour time point. At one hour after infection, the media for each time point was changed to fresh
 450 influenza growth media. Note that the HA-expressing units were calculated without this additional
 451 washing step, and so likely represent an overestimate of our final infectious dose (consistent

452 with the fact that fewer than 30% of cells appear infected in the single-cell sequencing data). All
 453 cells were then harvested for single-cell analysis concurrently – ensuring all had spent equivalent
 454 time in changed media . For our replicate 8-hour time point, cells were infected as above except
 455 that the cells were infected at 0.1 HA-expressing units of virus per cell but no wash step was
 456 performed, and the sample was prepared on a different day. After harvest, cells were counted using
 457 disposable hemocytometers and diluted to equivalent concentrations with an intended capture
 458 of 3000 cells/sample following the manufacturer's provided by 10x Genomics for the Chromium
 459 Single Cell platform. All subsequent steps through library preparation followed the manufacturer's
 460 protocol. Samples were sequenced on an Illumina HiSeq. The deep sequencing data are available
 461 on the Sequence Read Archive under accession [*Upload in progress.*]

462 Computational analysis of single-cell mRNA sequencing data

463 Jupyter notebooks that perform all of the computational analyses are available in Supplemen-
 464 tary file 1 and at https://github.com/jbloomlab/flu_single_cell [*This GitHub repository will be made
 465 public upon acceptance of the manuscript. If you are a reviewer who needs access, please contact the
 466 editor.*].

467 Briefly, the raw deep sequencing data were processed using the 10X Genomics software package
 468 CellRanger (version 2.0.0). The reads were aligned to a concatenation of the human and influenza
 469 virus transcriptomes. The human transcriptome was generated by filtering genome assembly
 470 GRCh38 for protein coding genes defined in the GTF file GRCh38.87. The influenza virus transcrip-
 471 tome was generated from the reverse-complement of the wildtype WSN viral RNA sequences as
 472 encoded in the reverse-genetics plasmids (Figure 1-source data 1). CellRanger calls cells based on
 473 the number of observed cell barcodes, and creates a cell-gene matrix. We used custom Python
 474 code to annotate the cells in this matrix by the number of viral reads that could be assigned to
 475 the wildtype and synonymously barcoded virus. Only about half of the viral reads overlapped
 476 the barcoded regions of the genes (Figure 1A) and could therefore be assigned to a viral barcode
 477 (Figure 4-Figures supplement 1). So for calculations of the number of reads in a cell derived from
 478 each viral barcode for each viral gene, the total number of detected molecules of that gene are
 479 multiplied by the fraction of those molecules with assignable barcodes that are assigned to that
 480 barcode. This annotated cell-gene matrix is in Supplementary file 2. A Jupyter notebook that
 481 performs these analyses is in Supplementary file 1.

482 The annotated cell-gene matrix was analyzed in R, primarily using the Monocle package (version
 483 2.4.0) (*Qiu et al., 2017; Trapnell et al., 2014*). A Jupyter notebook that performs these analyses is in
 484 Supplementary file 1. For each sample, cell barcodes that had >2.5-fold fewer or more UMI counts
 485 mapping to cellular transcripts than the sample mean were excluded from downstream analyses
 486 (see red vertical lines in Figure 3B).

487 In order to determine an appropriate cutoff for how many reads a cell needed to contain in
 488 order to be classified as infected, we calculated the mean viral barcode purity across all cells that
 489 contained at least a given fraction of viral mRNA and had multiple viral reads that could be assigned
 490 a barcode (Figure 4B,C and Figure 4-Figure supplement 2). We then determined the threshold
 491 fraction of viral mRNA at which the mean purity no longer increased as a function of the amount
 492 of viral mRNA. This threshold represents the point at which we have effectively eliminated cells
 493 that have low barcode purity simply due to lysis-acquired reads sampled randomly from both viral
 494 barcodes. As is apparent from Figure 4B, only the 10-hour sample and the 8-hour-2 sample have
 495 the excess of mixed barcodes among cells with low amounts of viral mRNA. The likely reason is that
 496 these samples have more total viral mRNA (and so there is more available mRNA to be acquired
 497 from lysed cells); in addition, there is always some experimental variability in the amount of cell
 498 lysis during the 10X sequencing process, and these samples may simply have the most. So the
 499 above threshold procedure is appropriate for those two samples. For the other samples, we simply
 500 set a minimum threshold of requiring at least a fraction 2×10^{-4} reads to come from viral mRNA as
 501 explained in the legend to Figure 4-Figure supplement 2. The thresholds for each sample are shown

502 in Figure 4C and Figure 4-Figure supplement 2. This procedure is expected to be conservative, and
 503 may miss some truly infected cells with very low amounts of viral mRNA. For subsequent analyses,
 504 we retained all infected cells and a subsample of uninfected cells (the greater of 50 or the number
 505 of infected cells for that sample). The rationale for subsampling the uninfected cell is that the
 506 vast majority of cells are uninfected, and we did not want these cells to completely dominate the
 507 downstream analyses. Cells were classified as co-infected if both viral variants had an RNA level
 508 that exceeded the threshold, and if the minor variant contributed at least 5% of the viral mRNA.

509 For the semi-supervised t-SNE clustering, we used Monocle's cell hierarchy function to bin cells
 510 into those with no viral mRNA, <2% viral mRNA, between 2% and 20% viral mRNA, and >20%.
 511 Candidate marker genes for t-SNE dimensionality reduction were then determined using the
 512 Monocle function markerDiffTable, excluding the effects of sample variation and the number of
 513 genes identified in a given cell, using a q-value cutoff of 0.01. The specificity of these markers was
 514 determined using the function calculateMarkerSpecificity – the top 50 markers were retained, and
 515 used to place populations in a two-dimensional plane based on tSNE dimensionality reduction.

516 For the analyses of cellular genes that differed in expression as a function of the amount of viral
 517 mRNA, we only considered cells that expressed all 8 viral mRNAs to avoid effects driven simply by
 518 viral gene absence. We also only considered cellular genes in the differential gene analysis, since
 519 viral gene expression will tautologically co-vary with the amount of viral mRNA. Additionally, because
 520 influenza virus has the capacity to degrade or prevent the synthesis of host mRNAs (*Bercovich-*
Kinori et al., 2016) and contributes significantly to the total number UMIs in some cells, we calculate
 521 size factors (a scalar value representing efficiency of UMI capture) based on cellular transcripts alone.
 522 Finally, we assigned all cells a ceiling fraction of mRNA from virus of 25% so that a few extremely
 523 high-expressing cells did not dominate. Cellular genes with expression that co-varied with the
 524 fraction of viral mRNAs in a cell were then determined using the Monocle differentialGeneTest, after
 525 removing variance explained by sample to sample variation. Figure 9 shows all genes that were
 526 significantly associated with the fraction of mRNA from virus at a false discovery rate of 0.1.
 527

528 Acknowledgments

529 We thank Xiaojie Qiu for advice about use of the Monocle software package, David Bacsik and
 530 Robert Bradley for comments on the manuscript, and the Fred Hutch Genomics Core for performing
 531 the Illumina deep sequencing.

532 References

- 533 **Aguilera ER**, Erickson AK, Jesudhasan PR, Robinson CM, Pfeiffer JK. Plaques formed by mutagenized viral
populations have elevated coinfection frequencies. *mBio*. 2017; 8(2):e02020.
- 535 **Akpınar F**, Timm A, Yin J. High-Throughput Single-Cell Kinetics of Virus Infections in the Presence of Defective
Interfering Particles. *Journal of Virology*. 2016 Jan; 90(3):1599–1612.
- 537 **Amatore D**, Sgarbanti R, Aquilano K, Baldelli S, Limongi D, Civitelli L, Nencioni L, Garaci E, Ciriolo MR, Palamara
AT. Influenza virus replication in lung epithelial cells depends on redox-sensitive pathways activated by
NOX4-derived ROS. *Cellular microbiology*. 2014 Oct; 17(1):131–145.
- 540 **Avraham R**, Haseley N, Brown D, Penaranda C, Jijon HB, Trombetta JJ, Satija R, Shalek AK, Xavier RJ, Regev A, et al.
Pathogen cell-to-cell variability drives heterogeneity in host immune responses. *Cell*. 2015; 162(6):1309–1321.
- 542 **Banning A**, Deubel S, Kluth D, Zhou Z, Brigelius-Flohe R. The GI-GPx Gene Is a Target for Nrf2. *Molecular and
Cellular Biology*. 2005 May; 25(12):4914–4923.
- 544 **Bercovich-Kinori A**, Tai J, Gelbart IA, Shitrit A, Ben-Moshe S, Drori Y, Itzkovitz S, Mandelboim M, Stern-Ginossar
N. A systematic view on influenza induced host shutoff. *eLife*. 2016 Aug; 5:e18311.
- 546 **Bhushal S**, Wolfsmüller M, Selvakumar TA, Kemper L, Wirth D, Hornef MW, Hauser H, Köster M. Cell polarization
and epigenetic status shape the heterogeneous response to Type III interferons in intestinal epithelial cells.
Frontiers in immunology. 2017; 8:671.

- 549 **Bloom JD.** An experimentally determined evolutionary model dramatically improves phylogenetic fit. *Molecular
550 Biology and Evolution.* 2014; 31(8):1956–1978.
- 551 **Brooke CB, Ince WL, Wrammert J, Wrammert J, Ahmed R, Wilson PC, Bennink JR, Yewdell JW.** Most Influenza A
552 Virions Fail To Express at Least One Essential Viral Protein. *Journal of Virology.* 2013 Feb; 87(6):3155–3162.
- 553 **Brooke CB.** Biological activities of ‘noninfectious’ influenza A virus particles. *Future Virology.* 2014 Jan; 9(1):41–51.
- 554 **Brooke CB, Ince WL, Wei J, Bennink JR, Yewdell JW.** Influenza A virus nucleoprotein selectively decreases
555 neuraminidase gene-segment packaging while enhancing viral fitness and transmissibility. *Proceedings of
556 the National Academy of Sciences.* 2014; 111(47):16854–16859.
- 557 **Buganim Y, Faddah DA, Cheng AW, Itsikovich E, Markoulaki S, Ganz K, Klemm SL, van Oudenaarden A, Jaenisch R.**
558 Single-cell expression analyses during cellular reprogramming reveal an early stochastic and a late hierachic
559 phase. *Cell.* 2012; 150(6):1209–1222.
- 560 **Cai L, Friedman N, Xie XS.** Stochastic protein expression in individual cells at the single molecule level. *Nature.*
561 2006; 440(7082):358–362.
- 562 **Cao J, Packer JS, Ramani V, Cusanovich DA, Huynh C, Daza R, Qiu X, Lee C, Furlan SN, Steemers FJ, et al.**
563 Comprehensive single-cell transcriptional profiling of a multicellular organism. *Science.* 2017; 357(6352):661–
564 667.
- 565 **Chen S, Chen S, Short JAL, Young DF, Killip MJ, Schneider M, Schneider M, Goodbourn S, Randall RE.** Heterocellular
566 induction of interferon by negative-sense RNA viruses. *Virology.* 2010 Nov; 407(2):247–255.
- 567 **Chua MA, Schmid S, Perez JT, Langlois RA, et al.** Influenza A virus utilizes suboptimal splicing to coordinate the
568 timing of infection. *Cell reports.* 2013; 3(1):23–29.
- 569 **Combe M, Garijo R, Geller R, Cuevas JM, Sanjuán R.** Single-cell analysis of RNA virus infection identifies multiple
570 genetically diverse viral genomes within single infectious units. *Cell host & microbe.* 2015; 18(4):424–432.
- 571 **Crotta S, Davidson S, Mahlakoiv T, Desmet CJ, Buckwalter MR, Albert ML, Staeheli P, Wack A.** Type I and type III
572 interferons drive redundant amplification loops to induce a transcriptional signature in influenza-infected
573 airway epithelia. *PLoS Pathogens.* 2013; 9(11):e1003773.
- 574 **Delbrück M.** The burst size distribution in the growth of bacterial viruses (bacteriophages). *Journal of bacteriology.*
575 1945 Aug; 50(2):131–135.
- 576 **Dimmock NJ, Dimmock NJ, Easton AJ, Easton AJ.** Defective Interfering Influenza Virus RNAs: Time To Reevaluate
577 Their Clinical Potential as Broad-Spectrum Antivirals? *Journal of Virology.* 2014 Apr; 88(10):5217–5227.
- 578 **Dou D, Hernández-Neuta I, Wang H, Östbye H, Qian X, Thiele S, Resa-Infante P, Kouassi NM, Sender V, Henrich K,
579 Mellroth P, Henriques-Normark B, Gabriel G, Nilsson M, Daniels R.** Analysis of IAV Replication and Co-infection
580 Dynamics by a Versatile RNA Viral Genome Labeling Method. *Cell reports.* 2017 Jul; 20(1):251–263.
- 581 **Doud M, Bloom J.** Accurate Measurement of the Effects of All Amino-Acid Mutations on Influenza Hemagglutinin.
582 *Viruses.* 2016 Jun; 8(6):155–17.
- 583 **Doud MB, Hensley SE, Bloom JD.** Complete mapping of viral escape from neutralizing antibodies. *PLoS
584 Pathogens.* 2017 Mar; 13(3):e1006271.
- 585 **Doyle V, Virji S, Crompton M.** Evidence that cyclophilin-A protects cells against oxidative stress. *The Biochemical
586 journal.* 1999 Jul; 341 (Pt 1)(Pt 1):127–132.
- 587 **Dubois J, Terrier O, Rosa-Calatrava M.** Influenza viruses and mRNA splicing: doing more with less. *MBio.* 2014;
588 5(3):e00070–14.
- 589 **Duong HQ, You K, Oh S, Kwak SJ, Seong YS.** Silencing of NRF2 Reduces the Expression of ALDH1A1 and ALDH3A1
590 and Sensitizes to 5-FU in Pancreatic Cancer Cells. *Antioxidants.* 2017 Sep; 6(3):52–10.
- 591 **Eisfeld AJ, Neumann G, Kawaoka Y.** At the centre: influenza A virus ribonucleoproteins. *Nature reviews
592 Microbiology.* 2015; 13(1):28.
- 593 **Elowitz MB, Levine AJ, Siggia ED, Swain PS.** Stochastic gene expression in a single cell. *Science.* 2002;
594 297(5584):1183–1186.

- 595 **Fensterl V**, Sen GC. The ISG56/IFIT1 gene family. *Journal of Interferon & Cytokine Research*. 2011 Jan; 31(1):71–78.
- 597 **Fonville JM**, Marshall N, Tao H, Steel J, Lowen AC. Influenza Virus Reassortment Is Enhanced by Semi-infectious Particles but Can Be Suppressed by Defective Interfering Particles. *PLoS Pathogens*. 2015 Oct; 11(10):e1005204.
- 600 **García-Sastre A**, Egorov A, Matassov D, Brandt S, Levy DE, Durbin JE, Palese P, Muster T. Influenza A virus lacking the NS1 gene replicates in interferon-deficient systems. *Virology*. 1998; 252(2):324–330.
- 602 **Geiss GK**, Salvatore M, Tumpey TM, Carter VS, Wang X, Basler CF, Taubenberger JK, Bumgarner RE, Palese P, Katze MG, García-Sastre A. Cellular transcriptional profiling in influenza A virus-infected lung epithelial cells: the role of the nonstructural NS1 protein in the evasion of the host innate defense and its potential contribution to pandemic influenza. *Proceedings of the National Academy of Sciences of the United States of America*. 2002 Aug; 99(16):10736–10741.
- 607 **Gorrini C**, Harris IS, Mak TW. Modulation of oxidative stress as an anticancer strategy. *Nature Publishing Group*. 2013 Dec; 12(12):931–947.
- 609 **Hagai T**, Chen X, Miragaia RJ, Gomes T, Rostom R, Kunowska N, Proserpio V, Donati G, Bossini-Castillo L, Naamati G, Emerton G, Trynka G, Kondova I, Denis M, Teichmann SA. Gene expression variability across cells and species shapes innate immunity. *bioRxiv*. 2017; doi: 10.1101/137992.
- 612 **Hale BG**, Randall RE, Ortín J, Jackson D. The multifunctional NS1 protein of influenza A viruses. *Journal of General Virology*. 2008; 89(10):2359–2376.
- 614 **Hatada E**, Hasegawa M, Mukaigawa J, Shimizu K, Fukuda R. Control of influenza virus gene expression: quantitative analysis of each viral RNA species in infected cells. *The Journal of Biochemistry*. 1989; 105(4):537–546.
- 616 **Heldt FS**, Frensing T, Reichl U. Modeling the intracellular dynamics of influenza virus replication to understand the control of viral RNA synthesis. *Journal of Virology*. 2012; 86(15):7806–7817.
- 618 **Heldt FS**, Kupke SY, Dorl S, Reichl U, Frensing T. Single-cell analysis and stochastic modelling unveil large cell-to-cell variability in influenza A virus infection. *Nature communications*. 2015 Nov; 6:1–12.
- 620 **Hoffmann E**, Stech J, Guan Y, Webster RG, Perez DR. Universal primer set for the full-length amplification of all influenza A viruses. *Archives of virology*. 2001 Dec; 146(12):2275–2289.
- 622 **Hoffmann E**, Neumann G, Kawacka Y, Hobom G, Webster RG. A DNA transfection system for generation of influenza A virus from eight plasmids. *Proceedings of the National Academy of Sciences*. 2000; 97(11):6108–6113.
- 625 **Huang AS**, Baltimore D, et al. Defective viral particles and viral disease processes. *Nature*, London. 1970; 226:325–7.
- 627 **Huang IC**, Li W, Sui J, Marasco W, Choe H, Farzan M. Influenza A Virus Neuraminidase Limits Viral Superinfection. *Journal of Virology*. 2008 Apr; 82(10):4834–4843.
- 629 **Huang T**, Palese P, Krystal M. Determination of influenza virus proteins required for genome replication. *Journal of Virology*. 1990; 64(11):5669–5673.
- 631 **Hutchinson EC**, von Kirchbach JC, Gog JR, Digard P. Genome packaging in influenza A virus. *Journal of general virology*. 2010; 91(2):313–328.
- 633 **Iwasaki A**, Pillai PS. Innate immunity to influenza virus infection. *Nature Reviews Immunology*. 2014 May; 14(5):315–328.
- 635 **Jiang X**, An Z, Lu C, Chen Y, Du E, Qi S, Yang K, Zhang Z, Xu Y. The protective role of Nrf2-Gadd45b against antimony-induced oxidative stress and apoptosis in HEK293 cells. *Toxicology Letters*. 2016 Aug; 256:11–18.
- 637 **Jung KA**, Lee S, Kwak MK. NFE2L2/NRF2 Activity Is Linked to Mitochondria and AMP-Activated Protein Kinase Signaling in Cancers Through miR-181c/Mitochondria-Encoded Cytochrome C Oxidase Regulation. *Antioxidants & Redox Signaling*. 2017 Apr; p. ars.2016.6797–3.
- 640 **Kallfass C**, Lienenklaus S, Weiss S, Staeheli P. Visualizing the beta interferon response in mice during infection with influenza A viruses expressing or lacking nonstructural protein 1. *Journal of Virology*. 2013 Jun; 87(12):6925–6930.

- 643 **Killip MJ**, Jackson D, Perez-Cidoncha M, Fodor E, Randall RE. Single-cell studies of IFN- β promoter activation by
644 wild-type and NS1-defective influenza A viruses. *Journal of General Virology*. 2017 Mar; 98(3):357–363.
- 645 **Killip MJ**, Smith M, Jackson D, Randall RE. Activation of the Interferon Induction Cascade by Influenza A Viruses
646 Requires Viral RNA Synthesis and Nuclear Export. *Journal of Virology*. 2014 Mar; 88(8):3942–3952.
- 647 **Killip MJ**, Fodor E, Randall RE. Influenza virus activation of the interferon system. *Virus research*. 2015 Feb; .
- 648 **Kim KH**, Jeong JY, Surh YJ, Kim KW. Expression of stress-response ATF3 is mediated by Nrf2 in astrocytes. *Nucleic
649 Acids Research*. 2009 Oct; 38(1):48–59.
- 650 **Klein AM**, Mazutis L, Akartuna I, Tallapragada N, Veres A, Li V, Peshkin L, Weitz DA, Kirschner MW. Droplet
651 Barcodeing for Single-Cell Transcriptomics Applied to Embryonic Stem Cells. *Cell*. 2015 May; 161(5):1187–1201.
- 652 **Lauring AS**, Andino R. Quasispecies Theory and the Behavior of RNA Viruses. *PLoS Pathogens*. 2010 Jul;
653 6(7):e1001005–8.
- 654 **Le Meur N**, Hahne F, Ellis B, Haaland P. FlowCore: data structures package for flow cytometry data. *Bioconductor
655 Project*; 2007.
- 656 **Lee D**, Ryu KY. Effect of cellular ubiquitin levels on the regulation of oxidative stress response and proteasome
657 function via Nrf1. *Biochemical and Biophysical Research Communications*. 2017 Apr; 485(2):234–240.
- 658 **Leonard AS**, Weissman D, Greenbaum B, Ghedin E, Koelle K. Transmission Bottleneck Size Estimation from
659 Pathogen Deep-Sequencing Data, with an Application to Human Influenza A Virus. *Journal of Virology*. 2017;
660 p. JVI-00171–17.
- 661 **Lin X**, Wang R, Zou W, Sun X, Liu X, Zhao L, Wang S, Jin M. The Influenza Virus H5N1 Infection Can Induce ROS
662 Production for Viral Replication and Host Cell Death in A549 Cells Modulated by Human Cu/Zn Superoxide
663 Dismutase (SOD1) Overexpression. *Viruses*. 2016 Jan; 8(1):13–16.
- 664 **Lopez CB**. Defective Viral Genomes: Critical Danger Signals of Viral Infections. *Journal of Virology*. 2014 Jul;
665 88(16):8720–8723.
- 666 **Van der Maaten L**, Hinton G. Visualizing data using t-SNE. *Journal of Machine Learning Research*. 2008;
667 9:2579–2605.
- 668 **MacLeod AK**, Acosta-Jimenez L, Coates PJ, McMahon M, Carey FA, Honda T, Henderson CJ, Wolf CR. Aldo-keto
669 reductases are biomarkers of NRF2 activity and are co-ordinately overexpressed in non-small cell lung cancer.
670 *British journal of cancer*. 2016 Dec; 115(12):1530–1539.
- 671 **Macosko EZ**, Basu A, Satija R, Nemesh J, Shekhar K, Goldman M, Tirosh I, Bialas AR, Kamitaki N, Martersteck EM,
672 et al. Highly parallel genome-wide expression profiling of individual cells using nanoliter droplets. *Cell*. 2015;
673 161(5):1202–1214.
- 674 **von Magnus P**. Incomplete forms of influenza virus. *Advances in Virus Research*. 1954; 2:59–79.
- 675 **Marsh GA**, Hatami R, Palese P. Specific residues of the influenza A virus hemagglutinin viral RNA are important
676 for efficient packaging into budding virions. *Journal of Virology*. 2007; 81(18):9727–9736.
- 677 **McCrone JT**, Woods RJ, Martin ET, Malosh RE, Monto AS, Lauring AS. Stochastic processes dominate the within
678 and between host evolution of influenza virus. *bioRxiv*. 2017; p. 176362.
- 679 **Miura T**, Taketomi A, Nishinaka T, Terada T. Regulation of human carbonyl reductase 1 (CBR1, SDR21C1) gene
680 by transcription factor Nrf2. *Chemico-Biological Interactions*. 2013 Feb; 202(1–3):126–135.
- 681 **Murray J**, Taylor SW, Zhang B, Ghosh SS, Capaldi RA. Oxidative Damage to Mitochondrial Complex I Due to
682 Peroxynitrite. *Journal of Biological Chemistry*. 2003 Sep; 278(39):37223–37230.
- 683 **Neumann G**, Watanabe T, Ito H, Watanabe S, Goto H, Gao P, Hughes M, Perez DR, Donis R, Hoffmann E, Hobom
684 G, Kawaoka Y. Generation of influenza A viruses entirely from cloned cDNAs. *Proceedings of the National
685 Academy of Sciences of the United States of America*. 1999 Aug; 96(16):9345–9350.
- 686 **Nobusawa E**, Sato K. Comparison of the mutation rates of human influenza A and B viruses. *Journal of Virology*.
687 2006; 80(7):3675–3678.
- 688 **Noda T**, Sagara H, Yen A, Takada A, Kida H, Cheng RH, Kawaoka Y. Architecture of ribonucleoprotein complexes
689 in influenza A virus particles. *Nature*. 2006; 439(7075):490.

- 690 **Parvin JD**, Moscona A, Pan W, Leider J, Palese P. Measurement of the mutation rates of animal viruses: influenza
691 A virus and poliovirus type 1. *Journal of Virology*. 1986; 59(2):377–383.
- 692 **Pauly MD**, Procario MC, Lauring AS. A novel twelve class fluctuation test reveals higher than expected mutation
693 rates for influenza A viruses. *eLife*. 2017; 6:e26437.
- 694 **Perez JT**, Varble A, Sachidanandam R, Zlatev I, Manoharan M, García-Sastre A, et al. Influenza A virus-generated
695 small RNAs regulate the switch from transcription to replication. *Proceedings of the National Academy of
696 Sciences*. 2010; 107(25):11525–11530.
- 697 **Perez-Cidoncha M**, Killip MJ, Oliveros JC, Asensio VJ, Fernandez Y, Bengoechea JA, Randall RE, Ortín J. An
698 Unbiased Genetic Screen Reveals the Polygenic Nature of the Influenza Virus Anti-Interferon Response.
699 *Journal of Virology*. 2014 Apr; 88(9):4632–4646.
- 700 **Peuchant E**, Bats ML, Moranvillier I, Lepoivre M, Guittot J, Wendum D, Lacombe ML, Moreau-Gaudry F, Boissan
701 M, Dabernat S. Metastasis suppressor NM23 limits oxidative stress in mammals by preventing activation of
702 stress-activated protein kinases/JNKs through its nucleoside diphosphate kinase activity. *The FASEB Journal*.
703 2017 Mar; 31(4):1531–1546.
- 704 **Poon LL**, Song T, Rosenfeld R, Lin X, Rogers MB, Zhou B, Sebra R, Halpin RA, Guan Y, Twaddle A, DePasse JV,
705 Stockwell TB, Wentworth DE, Holmes EC, Greenbaum B, Peiris JSM, Cowling BJ, Ghedin E. Quantifying influenza
706 virus diversity and transmission in humans. *Nature Genetics*. 2016; 48(2):195–200.
- 707 **Qiu X**, Mao Q, Tang Y, Wang L, Chawla R, Pliner HA, Trapnell C. Reversed graph embedding resolves complex
708 single-cell trajectories. *Nature Methods*. 2017 Aug; p. 1–10.
- 709 **Raj A**, Peskin CS, Tranchina D, Vargas DY, Tyagi S. Stochastic mRNA synthesis in mammalian cells. *PLoS Biology*.
710 2006; 4(10):e309.
- 711 **Rand U**, Rinas M, Schwerk J, Nöhren G, Linnes M, Kröger A, Flossdorf M, Kullai KK, Hauser H, Höfer T, Köster M.
712 Multi-layered stochasticity and paracrine signal propagation shape the type-I interferon response. *Molecular
713 Systems Biology*. 2012 Jan; 8(1):584.
- 714 **Reed LJ**, Muench H. A simple method of estimating fifty percent endpoints. *American journal of epidemiology*.
715 1938; 27(3):493–497.
- 716 **Saira K**, Lin X, DePasse JV, Halpin R, Twaddle A, Stockwell T, Angus B, Cozzi-Lepri A, Delfino M, Dugan V, Dwyer
717 DE, Freiberg M, Horban A, Losso M, Lynfield R, Wentworth DN, Holmes EC, Davey R, Wentworth DE, Ghedin E.
718 Sequence analysis of in vivo defective interfering-like RNA of influenza A H1N1 pandemic virus. *Journal of
719 Virology*. 2013; 87(14):8064–8074.
- 720 **Schulte MB**, Andino R. Single-Cell Analysis Uncovers Extensive Biological Noise in Poliovirus Replication. *Journal
721 of Virology*. 2014 May; 88(11):6205–6212.
- 722 **Sgarbanti R**, Amatore D, Celestino I, Marcocci ME, Fraternale A, Ciriolo MR, Magnani M, Saladino R, Garaci E,
723 Palamara AT, Nencioni L. Intracellular redox state as target for anti-influenza therapy: are antioxidants always
724 effective? *Current topics in medicinal chemistry*. 2014; 14(22):2529–2541.
- 725 **Shalek AK**, Satija R, Adiconis X, Gertner RS, Gaublomme JT, Raychowdhury R, Schwartz S, Yosef N, Malboeuf C,
726 Lu D, et al. Single-cell transcriptomics reveals bimodality in expression and splicing in immune cells. *Nature*.
727 2013; 498(7453):236–241.
- 728 **Shalek AK**, Satija R, Shuga J, Trombetta JJ, Gennert D, Lu D, Chen P, Gertner RS, Gaublomme JT, Yosef N, et al.
729 Single cell RNA Seq reveals dynamic paracrine control of cellular variation. *Nature*. 2014; 510(7505):363.
- 730 **Shapiro GI**, Gurney T, Krug RM. Influenza virus gene expression: control mechanisms at early and late times of
731 infection and nuclear-cytoplasmic transport of virus-specific RNAs. *Journal of Virology*. 1987 Mar; 61(3):764–
732 773.
- 733 **Suárez P**, Valcarcel J, Ortín J. Heterogeneity of the mutation rates of influenza A viruses: isolation of mutator
734 mutants. *Journal of Virology*. 1992; 66(4):2491–2494.
- 735 **Suárez-López P**, Ortín J. An estimation of the nucleotide substitution rate at defined positions in the influenza
736 virus haemagglutinin gene. *Journal of general virology*. 1994; 75(2):389–393.

- 737 **Sutejo R**, Yeo DS, Zu Myaing M, Hui C, Xia J, Ko D, Cheung PC, Tan BH, Sugrue RJ. Activation of Type I and III
738 Interferon Signalling Pathways Occurs in Lung Epithelial Cells Infected with Low Pathogenic Avian Influenza
739 Viruses. PLoS ONE. 2012; 7(3).
- 740 **Tapia K**, Kim Wk, Sun Y, Mercado-López X, Dunay E, Wise M, Adu M, López CB. Defective viral genomes arising
741 in vivo provide critical danger signals for the triggering of lung antiviral immunity. PLoS Pathogens. 2013;
742 9(10):e1003703.
- 743 **Trapnell C**, Cacchiarelli D, Grimsby J, Pokharel P, Li S, Morse M, Lennon NJ, Livak KJ, Mikkelsen TS, Rinn JL. The
744 dynamics and regulators of cell fate decisions are revealed by pseudotemporal ordering of single cells. Nature
745 Biotechnology. 2014 Mar; 32(4):381–386.
- 746 **Varble A**, Albrecht RA, Backes S, Crumiller M, Bouvier NM, Sachs D, García-Sastre A, et al. Influenza A virus
747 transmission bottlenecks are defined by infection route and recipient host. Cell host & microbe. 2014;
748 16(5):691–700.
- 749 **Vreede FT**, Jung TE, Brownlee GG. Model Suggesting that Replication of Influenza Virus Is Regulated by
750 Stabilization of Replicative Intermediates. Journal of Virology. 2004 Aug; 78(17):9568–9572.
- 751 **van der Walt S**, Colbert SC, Varoquaux G. The NumPy Array: A Structure for Efficient Numerical Computation.
752 Computing in Science & Engineering. 2017 Aug; 13(2):22–30.
- 753 **Xue J**, Chambers BS, Hensley SE, López CB. Propagation and Characterization of Influenza Virus Stocks That
754 Lack High Levels of Defective Viral Genomes and Hemagglutinin Mutations. Frontiers in microbiology. 2016
755 Mar; 7(Pt 10):e1004924–15.
- 756 **Xue KS**, Stevens-Ayers T, Campbell AP, Englund JA, Pergam SA, Boeckh M, Bloom JD. Parallel evolution of
757 influenza across multiple spatiotemporal scales. eLife. 2017 Jun; 6:e26875.
- 758 **Zheng GX**, Terry JM, Belgrader P, Ryvkin P, Bent ZW, Wilson R, Ziraldo SB, Wheeler TD, McDermott GP, Zhu J, et al.
759 Massively parallel digital transcriptional profiling of single cells. Nature communications. 2017; 8:14049.
- 760 **Zhu Y**, Yongky A, Yin J. Growth of an RNA virus in single cells reveals a broad fitness distribution. Virology. 2009;
761 385(1):39–46.

Supplementary file 1. Computer code for the analyses. This ZIP file contains a Jupyter notebook that runs CellRanger to align and annotate the reads, and a Jupyter notebook that uses Monocle to analyze the cell-gene matrix. The ZIP file also includes associated custom scripts.

Supplementary file 2. The annotated cell-gene matrix in Matrix Market Format. *[This file is too large for the eLife submission system. We will communicate with the editors to get it uploaded for a final accepted version, or we will post it on DataDryad. If you are a reviewer and need access, please contact the editor.]*

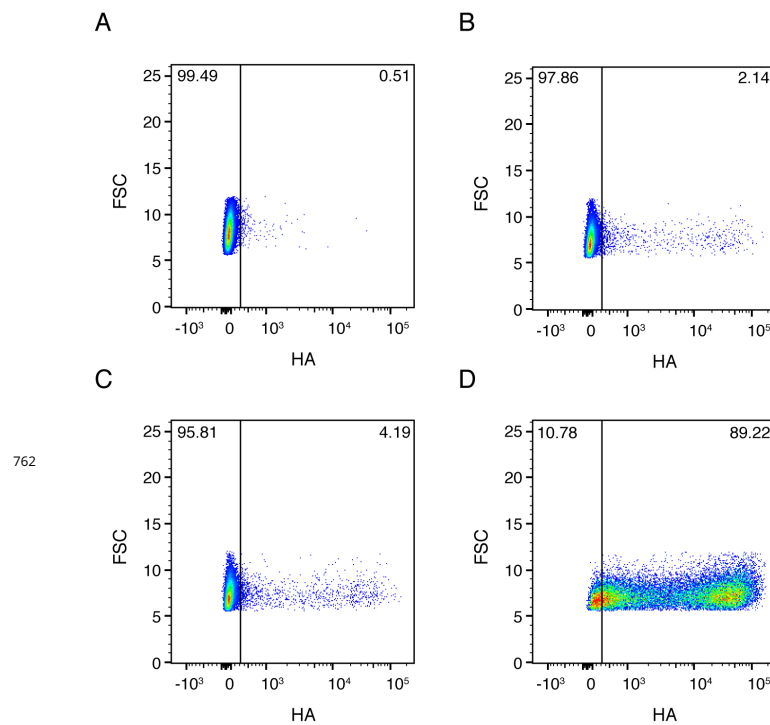


Figure 2–Figure supplement 1. Full flow cytometry data for Figure 2B. A549 cells were infected at an MOI of 0.1 as calculated by TCID₅₀ on MDCK-SIAT1 cells. **(A)** Uninfected gating control. **(B)** Cells infected with the wild-type virus stock used in our experiments. **(C)** Cells infected with synonymously barcoded virus stock used in our experiments. **(D)** Cells infected with a stock of wild-type virus propagated at a high MOI, and therefore enriched in defective particles.

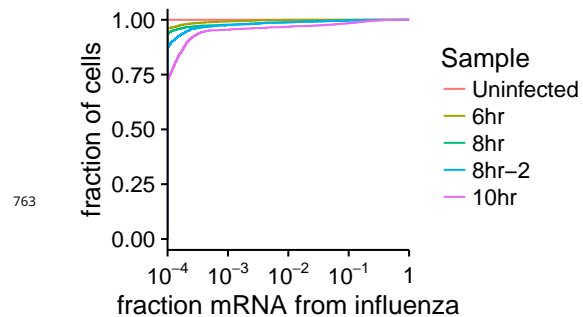


Figure 3–Figure supplement 1. For each sample, this plot shows the fraction of all cells that derive at least the indication fraction of their mRNA from influenza virus.

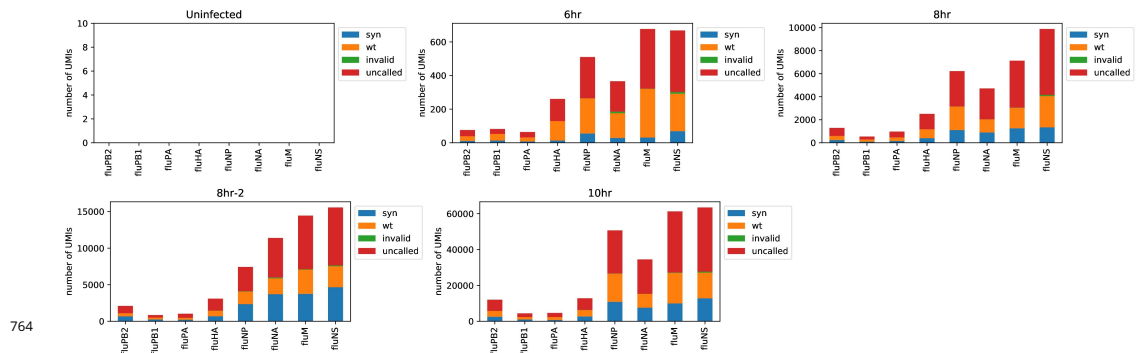


Figure 4-Figure supplement 1. The number of viral barcodes called for each sample and gene segment. Viral transcripts are classified as *syn* if they mapped to a synonymously barcoded influenza transcript, *wt* if they mapped to a wild-type influenza transcript, *invalid* if multiple reads for the same UMI differed on the status of the viral barcode, and as *uncalled* if none of the reads for that UMI overlapped the region of the viral transcript containing the viral barcode. For calculations of the number of reads in a cell derived from each viral barcode for each viral gene, the total number of detected molecules of that gene are multiplied by the fraction of those molecules with assignable barcodes that are assigned to that barcode.

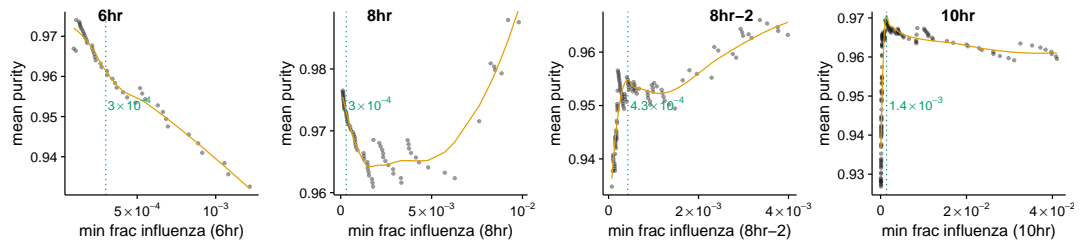


Figure 4-Figure supplement 2. Cell lysis can lead cells to the spurious association of small amounts of extraneous mRNA with individual cells. We wanted to avoid classifying as infected cells that had simply acquired such lysis-derived viral mRNA. The amount of lysis-derived viral mRNA will vary among samples as a function of both the lysis rate during the cell preparation (which always varies slightly from sample to sample in the 10X procedure) and with the amount of total viral mRNA for that sample (the more viral mRNA, the more there is to be acquired from lysed cells). As is shown in Figure 4B, the 8hr-2 and 10hr sample clearly have an enrichment of mixed barcodes in cells with small numbers of viral mRNA. For each sample, we calculated the mean purity of all cells with at least the indicated amount of viral mRNA, and determined the threshold amount of viral mRNA where purity no longer increased by finding the first maxima in a loess curve fit (orange line). We called the threshold at this point of maximum purity (dotted green line). For the 6hr and 8hr samples there is no indication of contamination from lysis-derived reads, as Figure 4B shows no increase in mixed barcodes in low viral mRNA cells. Therefore, for these samples we simply set a threshold of requiring at least 2×10^{-4} of the total mRNA to come from virus, which corresponds to ~ 2 viral mRNAs for the typical cell with 10^4 total reads (Figure 3B).

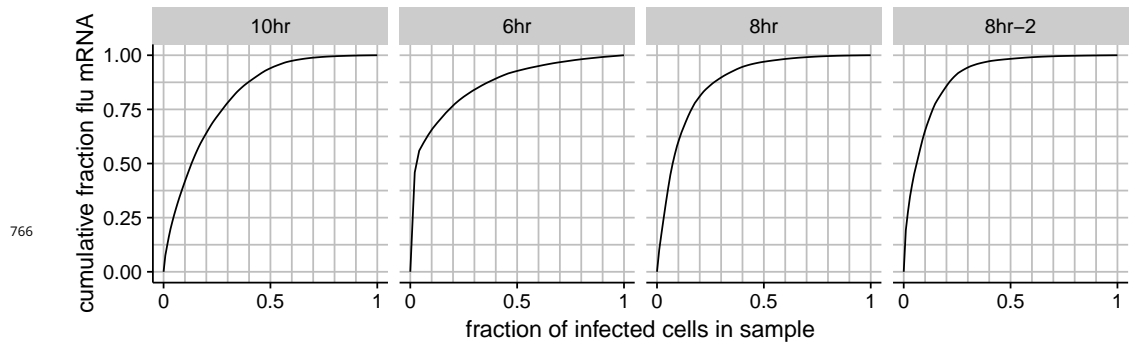


Figure 4-Figure supplement 3. The total fraction of all viral mRNA among infected cells that is attributable to a given fraction of these cells. For instance, the plot for the 8-hour sample shows that roughly 50% of all viral mRNA is derived from 10% of the infected cells.

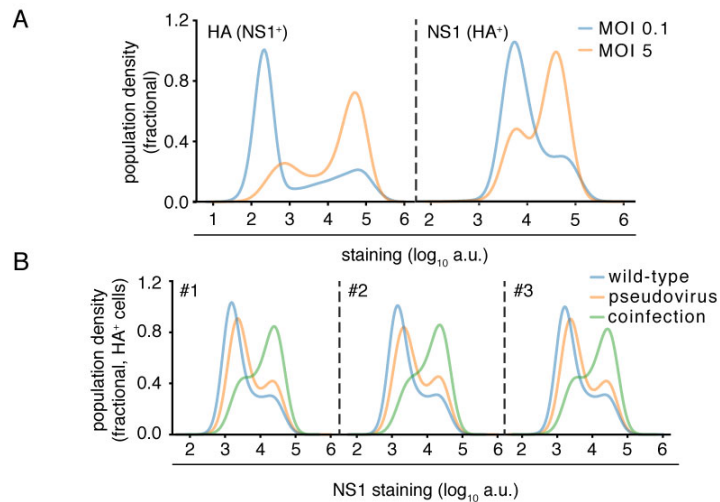


Figure 4-Figure supplement 4. (A) Expression of viral proteins in cells infected at high (MOI 5) as calculated by TCID50 on MDCK-SIAT1 cells) or low (MOI 0.1) initial infectious dose. Cells were concurrently stained for HA and NS1 proteins 10 hours post infection. HA staining was analyzed in cells positive for NS1 (left), and NS1 staining was analyzed in cells positive for HA (right). While a higher dose leads to more cells expressing high amounts of viral protein, it does not greatly increase the amount of viral protein in either the low-expressing or high-expressing cells. Therefore, higher viral dose does not lead to a large continuous increase in viral protein production among all cells – rather, it mostly changes the proportions of cells that fall in different parts of the highly heterogeneous distribution. **(B)** Cells were co-infected with a mix of wild-type virus and virus in which the HA gene was replaced by GFP flanked by the terminal regions of the HA gene segment at an MOI of 0.1 for each virus. At 10 hours post-infection, cells were stained for NS1 and HA expression and analyzed by flow cytometry. Cells could be annotated as infected by one or more infectious particles (wild-type or pseudovirus alone) or at least two infectious particles (coinfection). Coinfected cells, like cells infected at a higher infectious dose, occupy different positions in the distribution of viral protein production but do not exhibit a continuous increase in viral protein production. Replicates shown.

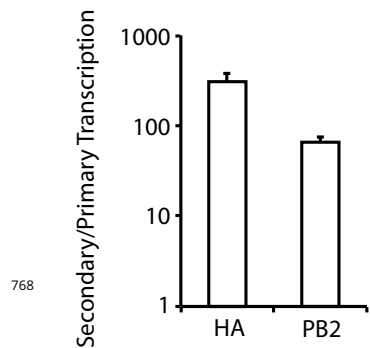


Figure 5–Figure supplement 1. A549 cells were infected at an MOI of 0.2 as calculated on MDCK-SIAT1 cells in either the presence or absence of the protein-translation inhibitor cyclohexamide, and viral mRNA was quantified at 8 hours post-infection by qPCR. The cyclohexamide prevents translation of new PB2, PB1, PA, and NP protein, and so prevents the formation of the new RNPs needed for secondary transcription. The bars show the relative amount of HA and PB2 mRNA in the absence versus the presence of cyclohexamide. Error \pm S.D. n=3.

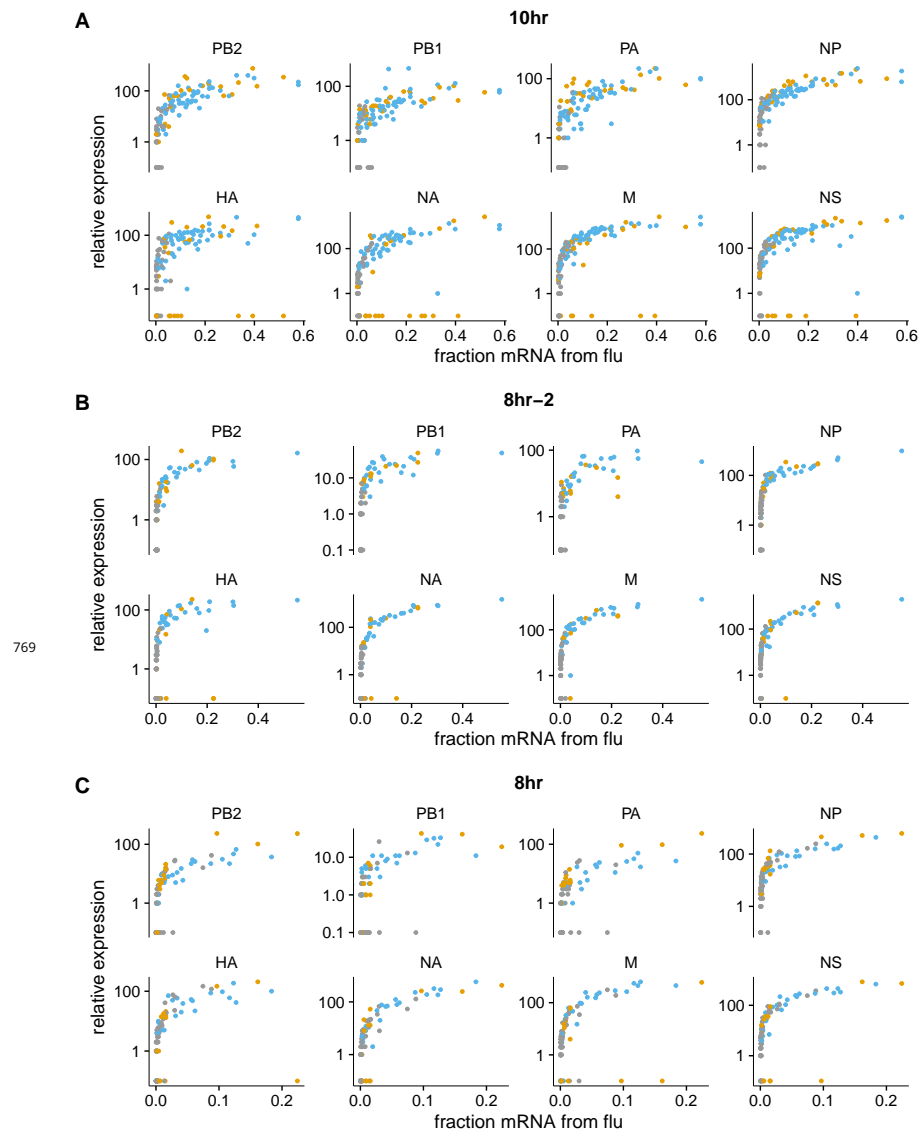


Figure 5–Figure supplement 2. The fraction of mRNA in each infected cell derived as a function of the normalized expression of each viral gene, shown for the 10-hour and 8-hour samples individually (the other samples had too few infected cells for this analysis to be useful). Points are colored as in Figure 5A.

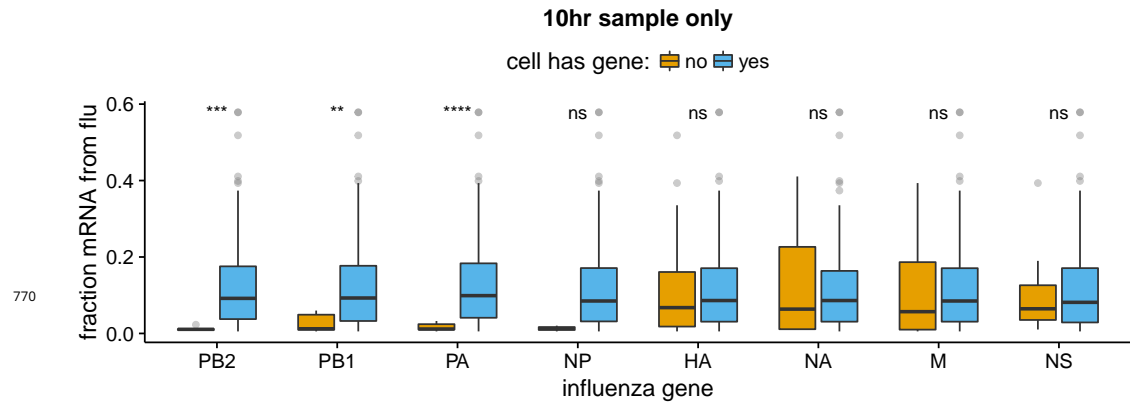


Figure 5–Figure supplement 3. The absence of viral RNP genes but *not* non-RNP genes remains significantly associated with reduced viral burden when we examine only the 10-hr sample, which is the single time point with the most data points. The difference for NP is no longer statistically significant due to low counts of infected cells lacking NP, but the trend remains. We do not show statistical analyses for other samples, as the number of infected cells is too low.

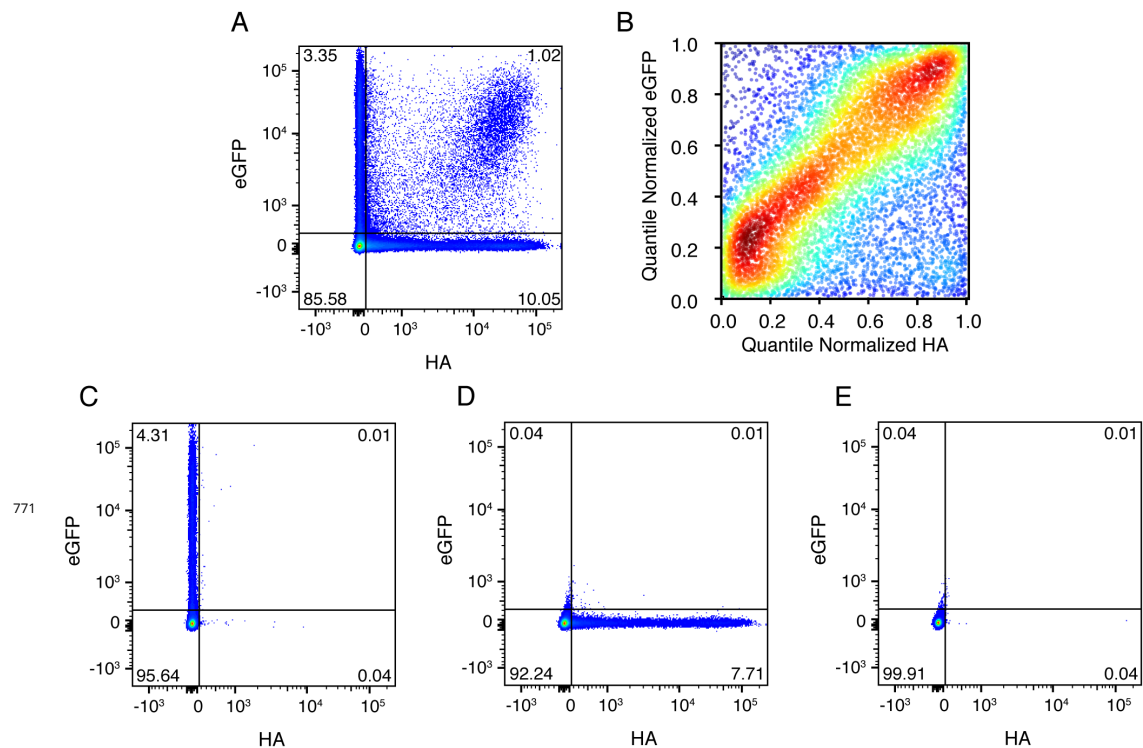


Figure 7–Figure supplement 1. **(A)** Cells were co-infected with a mix of wild-type virus and virus in which the HA gene was replaced by GFP flanked by the terminal regions of the HA gene segment. At 10 hours post-infection, cells were analyzed by flow cytometry for HA and eGFP expression. **(B)** The expression of HA and GFP are correlated in co-infected cells. Shown are the quantile-normalized HA and eGFP signals for double-positive cells. Cells are colored by density, using a Gaussian kernel density estimate. **(C),(D),(E)** Gating controls, single infection with eGFP virus, single infection with wild-type virus, and uninfected cells, respectively.

Category	Genes
Detoxification	AKR1C3, AKR1B10, GPX2, ALDH3A1, ALDH1A1, NQO1, CBR1, PRDX1
Protein folding	TXN, PPIA
Electron transport chain	NDUFB4, MT-CO1, MT-CO3
Regulators	ATF3, GADD45B
ROS-responsive relevance complex/unknown	UBB, NME1

Figure 9–Figure supplement 1. Table delineating genes in Figure 9 that are associated with the response to oxidative stress (*Duong et al., 2017; Jung et al., 2017; Lee and Ryu, 2017; Peuchant et al., 2017; MacLeod et al., 2016; Jiang et al., 2016; Gorrini et al., 2013; Miura et al., 2013; Kim et al., 2009; Banning et al., 2005; Murray et al., 2003; Doyle et al., 1999*).